

Evaluation of immune cell-specific functional response following single or combinatorial treatment with DNA damaging and immunotherapy agents using patient-derived immunocompetent cultures of High Grade Serous Ovarian Cancer

A Thesis submitted to

Indian Institute of Science Education and Research Pune in partial fulfilment of the requirements for the BS-MS Dual Degree Programme

by

Abhilash V A

20191189



Indian Institute of Science Education and Research Pune

Dr. Homi Bhabha Road,

Pashan, Pune 411008, INDIA.

Date: April, 2024

Under the guidance of
Supervisor: Dr Anniina Färkkilä, MD PhD,
Faculty of Medicine
University of Helsinki
TAC: Dr Satyajit Rath
Emeritus Professor
Department of Biology
IISER Pune

From June 2023 to Mar 2024

INDIAN INSTITUTE OF SCIENCE EDUCATION AND RESEARCH
PUNE

Certificate

This is to certify that this dissertation entitled “**Evaluation of immune cell-specific functional response following single or combinatorial treatment with DNA damaging and immunotherapy agents using patient-derived immunocompetent cultures of High Grade Serous Ovarian Cancer** ” towards the partial fulfilment of the BS-MS dual degree programme at the Indian Institute of Science Education and Research, Pune represents study/work carried out by **Abhilash V A** Institute of Science Education and Research under the supervision of **Dr Anniina Färkkilä, MD PhD** Assistant Professor, Faculty of Medicine, University of Helsinki during the academic year 2023-2024.

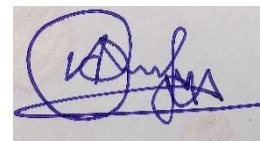
A handwritten signature in black ink, appearing to read 'A. Färkkilä', with a long horizontal stroke extending to the right.

Dr Anniina Färkkilä, MD PhD

This thesis is dedicated to my younger self, my family, my friends, and most of all, to the person who sat with me through it all.

Declaration

I hereby declare that the matter embodied in the report entitled “**Evaluation of immune cell-specific functional response following single or combinatorial treatment with DNA damaging and immunotherapy agents using patient-derived immunocompetent cultures of High Grade Serous Ovarian Cancer** ” are the results of the work carried out by me at Faculty of medicine, University of Helsinki under the supervision of **Dr Anniina Färkkilä, MD PhD** and the same has not been submitted elsewhere for any other degree



Abhilash V A

Date: 27.03.2024

Table of Contents

Certificate	3
Declaration	5
List of Tables	8
List of Figures	9
Acknowledgments	12
Introduction	14
High Grade Serous Ovarian cancer: Overview	14
Current treatment methods in HGSOC	15
Importance of DNA damage repair pathways in treatment	16
Immune microenvironment in HGSOC.....	17
Immunotherapy in Cancer Research and combining it with DNA damaging drugs.....	18
Immunocompetent cultures as a model system and preliminary results.....	20
Project Idea	23
Objectives	23
Materials	24
Buffers, reconstitutions and preparations.....	29
Methods	32
Sample collection, preparation, and storage.....	32
Organoid Culture (48 and 384 well plates).....	33
Media preparation	33
Organoid culture preparation and administration of drugs.....	33
Organoid dissociation	33
Flow Cytometry	34
Antibody staining.....	34
Single colour compensations.....	35
Immunofluorescence (384 well plates).....	35
Live/dye Staining	35
Antibody cocktail preparation	35
Antibody Staining and imaging.....	35
Data Analysis.....	36
FlowJO	36
CYTO	36
Cell Profiler	38

Results	39
Tumour tissue samples from 4 out of 14 patients were suitable for culturing in omentum gel	39
Immunocompetent cultures were established successfully from 3 patient-derived tumours	41
The immune cell population in the tumour tissue was recapitulated in the patient-derived immunocompetent cultures.....	42
Combination therapy of PARPi and anti PD1 antibody showed increased effector T cell proportion in the sample S321	43
CD8+ T cell functional activity was increased upon anti-PD1-antibody monotherapy and anti-PD1 antibody – PARPi combination therapy in sample S321	44
Decreased effector T cell proportions were observed with increased concentration of ATRi in samples S321 and S263.....	47
Decreased functional activity of CD8+ T cells exhibited a decline with increased concentration of ATRi	47
Highest effector T cell proportion in was seen in 0.2 µM ATXi concentration.....	50
Enhanced expression of GrzB was detected within CD8+ T cells in sample S321 following exposure to 0.2 µM of ATXi.....	50
Elevated proportions of CD8+ T cells were observed in samples S333 and S263 following administration of ATRi – ATXi combinations at higher concentrations	53
Functional activity of CD8+ T cells and CD11c+ cells was attenuated in combination therapies	53
Pronounced anti-tumour efficacy while maintaining minimal immune cell toxicity in the combinatorial treatment of 100 µM (ATRi) + 0.2 µM (ATXi).....	56
Discussion	59
References	62

List of Tables

Table 1: Reagents needed for base organoid media	24
Table 2: Interleukins needed for the complete organoid media	24
Table 3: Omentum culture constituents	25
Table 4: Drugs used in the experiments	25
Table 5: List of fluorochrome-tagged antibodies for surface antigens	26
Table 6: List of fluorochrome-tagged antibodies for intracellular antigens	26
Table 7: IF antibodies, their standardized concentrations	27
Table 8: List of medias used in the experiments	27
Table 9: Other solutions used in the experiments	28
Table 10: Miscellaneous items used in the experiments	28
Table 11: All the drug dilutions and combinations used for experiments.	31
Table 12: Samples collected and processed with Sample ID, site of origin, cells per ml, total number of cells	40

List of Figures

Figure 1: Current treatment plan for HGSOC patients (Nero et al., 2021b).	15
Figure 2: Mutations commonly seen in HGSOC patients. Most of these mutations are present in DNA damage response, repair, and cell cycle (Morand et al., 2021).	16
Figure 3: Immunophenotypes in HGSOC (Nero et al., 2021b).	18
Figure 4: Monotherapies and combination therapies of different classes of drugs on HGSOC iPDCs. The dot plot shows the action of different concentration of monotherapies of Olaparib (PARPi), Pembrolizumab (anti PD-1 antibody), Berzosertib (ATRI), Ziritaxestat (ATXi), AMG PERK 44 (PERKi), GSK3859856 (STING agonist) and Adavosertib (WEE1i), and their different combinations. Each dot is a particular treatment in a particular sample. The log ₂ FC shows the difference in the number of CK7+ (tumour) cells between control and each of the treatments. (unpublished data).	22
Figure 5: Tissue samples before the commencement of processing.	33
Figure 6: Settings used in CYTO to run each of the sample	37
Figure 7: Example showing Z scores of each immune cell marker per cluster	38
Figure 8: Immunocompetent cultures derived from Omental sample. Microscopy images of immunocompetent cultures on day 0 – A) 4X B) 10X C) 20X D) 40X and day 6 – E) 4X F) 10X G) 20X H) 40X	42
Figure 9: Immune cell proportion in the tumour tissue (day 0) and patient-derived immunocompetent cultures (day 3) from samples S321, S333 and S263. Each bar plot - S321, S333 and S263 shows the immune cell proportion obtained from flow cytometry on the day of tissue processing and the end of omentum gel culturing (post 72 hours). Proportions were obtained by clustering EpCam negative (non-tumour) cells using FlowSOM and annotated them using CYTO.	43
Figure 10: Immune cell proportion in the patient-derived immunocompetent cultures after treatment with 10 µg/ mL of pembrolizumab (anti PD1 antibody) or 20 µM Olaparib (PARPi) and their combination in samples S321, S333, S263. Each bar plot – S321, S333 and S263 shows the immune cell proportion obtained from flow cytometry on the day of tissue processing and the end of treatments (post 72 hours) with 10 µg/ mL of pembrolizumab (anti PD1 antibody) or 20 µM Olaparib (PARPi) and their combination. Proportions were obtained by clustering EpCam negative (non-tumour) cells using FlowSOM and annotated them using CYTO.	45
Figure 11: Immune cell Functional Activity of iPDCs of samples S321, S333 and S263 upon treatment with monotherapies of PARPi, Anti PD1 antibody and their combination. Treatment conditions performed were PARPi monotherapy – 20 µM of Olaparib (Ola) , anti-PD1-antibody monotherapy – 10 µg/ mL of Pembrolizumab (Pembro) and their combination (Ola + Pembro) . Functional activity of the immune cells were assessed by checking the levels of GrzB, IFN γ and Ki-67 for CD8+ T cells and IFN γ , Ki-67 and HLA-DR for CD11c+ cells. Each heatmap shows the log ₂ fold change of the immune cell functional markers for each cell type per treatment per sample.	46
Figure 12: Immune cell proportion in the patient-derived immunocompetent cultures after treatment with 0.02 µM, 0.1 µM and 1 µM of Berzosertib/ VE-822 (ATRI). Each bar plot – S321, S333 and S263 shows the immune cell proportion obtained from flow cytometry on the day of tissue processing and the end of treatments (post 72 hours) with 0.02 µM, 0.1 µM and 1 µM of Berzosertib/ VE-822 (ATRI) . Proportions were obtained by clustering EpCam negative (non-tumour) cells using FlowSOM and annotated them using CYTO.	48

Figure 13: Immune cell Functional Activity of iPDCs of samples S321, S333 and S263 on administering them with monotherapies of ATRi. Treatment conditions performed were ATRi monotherapy – 0.02 µM, 0.1 µM and 1 µM of Berzosertib/VE-822 (ATRi). Functional activity of the immune cells was assessed by checking the levels of GrzB, IFN γ and Ki-67 for CD8+ T cells and IFN γ , Ki-67 and HLA-DR for CD11c+ cells. Each heatmap shows the log2 fold change of the immune cell functional markers for each cell type per treatment per sample..... 49

Figure 14: Immune cell proportion in the patient-derived immunocompetent cultures after treatment with 0.13 µM, 0.2 µM and 0.7 µM of Ziritaxestat/ GLPG1690 (ATXi). Each bar plot – S321, S333 and S263, shows the immune cell proportion obtained from flow cytometry on the day of tissue processing and the end of treatments (post 72 hours) with 0.13 µM, 0.2 µM and 0.7 µM of Ziritaxestat/ GLPG1690 (ATXi). Proportions were obtained by clustering EpCam negative (non-tumour) cells using FlowSOM and annotated them using CYTO. 51

Figure 15: Immune cell Functional Activity of iPDCs of samples S321, S333 and S263 on administering them with monotherapies of ATXi. Treatment conditions performed were ATXi monotherapy – 0.13 µM, 0.2 µM and 0.7 µM of Ziritaxestat/ GLPG1690 (ATXi). (just the latter two for S263). Functional activity of the immune cells was assessed by checking the levels of GrzB, IFN γ and Ki-67 for CD8+ T cells and IFN γ , Ki-67 and HLA-DR for CD11c+ cells. Each heatmap shows the log2 fold change of the immune cell functional markers for each cell type per treatment per sample. 52

Figure 16: Immune cell proportion in the patient-derived immunocompetent cultures after treatment with combinations of Berzosertib/ VE-822 (ATRi) and Ziritaxestat/ GLPG1690 (ATXi). Each bar plot – S321, S333 and S263, shows the immune cell proportion obtained from flow cytometry on the day of tissue processing and the end of treatments (post 72 hours) with Combo 1 – ATRi 0.02 µM + ATXi 0.13 µM, Combo 2 – ATRi 0.1 µM + ATXi 0.2 µM, Combo 3 – ATRi 1 + ATXi 0.7, Combo 4 – ATRi 0.02 µM + ATXi 0.2 µM. Proportions were obtained by clustering EpCam negative (non-tumour) cells using FlowSOM and annotated them using CYTO. 54

Figure 17: Immune cell Functional Activity of iPDCs of samples S321, S333 and S263 on administering them with ATRi-ATXi combination therapies. Treatment conditions (all concentrations are in µM) performed were combinations of Berzosertib/ VE-822 (ATRi) and Ziritaxestat/ GLPG1690 (ATXi). Functional activity of the immune cells was assessed by checking the levels of GrzB, IFN γ and Ki-67 for CD8+ T cells and IFN γ , Ki-67 and HLA-DR for CD11c+ cells. Each heatmap shows the log2 fold change of the immune cell functional markers for each cell type per treatment per sample. 55

Figure 18: Boxplots showing proportion of CK7+ live cells normalised to control from iPDCs from S321, S333, S263. Treatment conditions (all concentrations are in µM) performed were monotherapy of Berzosertib/ VE-822 (ATRi) and Ziritaxestat/ GLPG1690 (ATXi) and their combinations. Tumour cell death was calculated using [CK7+ DCM+ cells/ all cells] from the intensities obtained from IF images. Each field in a well was taken as a single image and proportions for each of these images were calculated. *P<0.05, ***P<0.001..... 57

Figure 19: : Boxplots showing proportion of CD45+ live cells normalised to control from iPDCs from S321, S333, S263. Treatment conditions (all concentrations are in µM) performed were monotherapy of Berzosertib/ VE-822 (ATRi) and Ziritaxestat/ GLPG1690 (ATXi) and their combinations. Immune cell death was calculated using [CD45+ DCM+ cells/ all cells] from the intensities obtained from IF images. Each field in a well was taken as a single image and proportions for each of these images were calculated. ***P<0.001..... 58

Abstract

High Grade Serous Ovarian Cancer (HGSOC) is one of the most lethal gynaecological malignancies with a 5-year survival rate of less than 42%. Current treatment regimens against the disease include debulking surgeries, Neo Adjuvant Chemotherapy, and Poly (ADP-ribose) polymerase inhibitors. Immunotherapies have shown very little promise with regards to this disease. Here as part of a prospective clinical trial (OncosysOVA - NCT06117384), we use patient derived immunocompetent cultures (iPDCs) to test the efficacy and immune cell (CD8+ T cell, CD4+ T cell and CD11c+ T cell) functional activation using the markers : GrzB, IFN γ , Ki-67, HLA-DR upon treatment with a DNA damaging drug - Berzosertib/ VE-822 (ATRi) and novel immunotherapy drug - Ziritaxestat/ GLPG1690 (ATXi) drugs and their combination. Already established drugs such as Olaparib (PARPi) and Pembrolizumab (Anti-PD1-antibody) were used to validate the results obtained from the ATRi and ATXi treatments. The results showed that increased concentrations of both ATRi and ATXi are harmful for the immune cells and decreased the functional activity of these cells. A combination of ATRi 0.1 μ M + ATXi 0.2 μ M increased tumour cell death without having a pronounced immune cell death, while ATXi 0.2 treatment showed the highest immune cell activation. Most results were patient specific which adds more evidence to the usage of iPDCs for studying immune cell activity in the tumour infiltrated immune cells and as a pre-clinical tool to determine the treatment regimen and dosage for each patient.

Acknowledgments

I want to thank **Dr Anniina Färkkilä, MD PhD** for taking me in as a 5th-year project student and always being available to help me and guide me in the right direction. I would like to thank **Dr Ashwini Nagaraj** on helping through every step of the way. I also thank **Dr Satyajit Rath** for agreeing to be on my thesis advisory committee and giving me great advice and feedback in my mid-semester presentation.

I am grateful to **María M. Hincapié-Otero, Aditi Sirsikar, Saundarya Shah, Ada Junquera, Iga Niemiec, Fernando Perez, Matilda Salko, Angela Szabo, Inga-Maria Launonen, Aleksandra Shabanova, Ziqi Kang, Zhihan Liang** and **Minna Eriksson** for all the help, support, criticism, and advice provided during the period of the thesis.

I would like to thank **Ann Jewel Jude** for being my emotional pillar for this period and keeping me engaged in all the activities in the campus. I thank **Rose Mary Roshan** for tolerating my banter (thesis and off-thesis). I thank **Soham Deolankar** for being the best roommate (even across the seas). I thank **Sneha Jain** for keeping me entertained through the year with both offline and online contents.

I thank my batchmates **Hari, Nami, Maria, Adhi, Nived**, and others for being the best support system. I thank **Sidharth, Ananth, Pranav** and **Madhesh** for being the most amazing seniors I could hope for. I thank **KS, Suresh, Shijil, Ananthu, Joseph, Bhagi, Anuvind, Anwasha** and **Vikram** for being the most supportive juniors.

I thank **Indian Institute of Science Education and Research Pune**, for giving me an opportunity to be under the tutelage of an amazing group of professors. I am even more grateful for providing me with the greatest peer group I could have imagined.

Last but not least, I thank **Aji aunty** for being my first teacher and instilling in me a sense of inquisition. I thank **Papa, Amma, Appu** and **Kannettan** for being a constant sense of motivation to keep me pushing to pursue my aspirations. I thank all my uncles, aunts, grandparents, brothers and sisters for looking out for me, providing me with support in big and small ways. I could not have been here with even one of them missing.

Contributor name	Contributor role
Dr Anniina Färkkilä, Dr Ashwini Nagaraj	Conceptualization Ideas
Abhilash V A, Dr Ashwini Nagaraj	Methodology
Matilda Salko	Clinical Information
Abhilash V A, Aditi Sirsikar, Iga Niemiec	Software
Abhilash V A, Dr Ashwini Nagaraj	Validation
Abhilash V A, Dr Ashwini Nagaraj, Aditi Sirsikar	Formal analysis
Abhilash V A, Dr Ashwini Nagaraj	Investigation
Dr Anniina Färkkilä	Resources
Abhilash V A, Dr Ashwini Nagaraj	Data Curation
Abhilash V A	Writing - original draft preparation
Dr Ashwini Nagaraj, Dr Anniina Färkkilä	Writing - review and editing
Abhilash V A, Dr Ashwini Nagaraj	Visualization
Dr Anniina Färkkilä, Dr Ashwini Nagaraj	Supervision
Abhilash V A, Dr Ashwini Nagaraj, Dr Anniina Färkkilä	Project administration
Dr Anniina Färkkilä	Funding acquisition

Introduction

High Grade Serous Ovarian cancer: Overview

Of all the diseases plaguing humankind, cancer has always been a fatality that has made patients, doctors, and researchers equally helpless. Even though recent advancements in medicine have increased the survival rates of patients in the past decades, it is slowly growing into a global epidemic (Ugai et al., 2022). In 2020, 19.3 million patients were diagnosed with cancer compared to 17 million in 2018, with the total number of deaths increasing from 9.5 million to 10 million (Sung et al., 2021). Ovarian cancer is the 8th most common cancer and the 7th leading cause of cancer death worldwide in women, with a mortality rate of 57.9% (Jemal et al., 1999). The substantially higher mortality of the disease is closely associated with the absence of proper screening techniques, delayed onset of symptoms, and, most importantly, unresponsiveness to treatments (Nero et al., 2021a). Of this, High Grade Serous Ovarian Cancer (HGSOC) contributes to disproportionate fatalities, accounting for about two-thirds of the total Ovarian cancer death (Momenimovahed et al., 2019).

Recent findings suggest that the Fallopian tube is the origin of most HGSOC tumour mass (Perets et al., 2013). Since most patients (about 85%) are diagnosed with the disease quite late, the tumours are mostly in the later stages (III – IV) (*SEER Ovarian Cancer*, 2018). 96% of all HGSOC patients have *TP53* mutations, while 22% of them have *BRCA1/2* mutations (“Integrated Genomic Analyses of Ovarian Carcinoma,” 2011). Unlike most cancers, HGSOC does not metastasize through blood or lymph. Instead, they spread to adjacent organs in the peritoneal cavity through direct extension and/ or detachment of cancer cells from the primary tumour site (Lengyel, 2010). Accumulation of ascites fluid in the peritoneal cavity, which is an accompanying hallmark of HGSOC, aids in this spread (Meza-Perez & Randall, 2017). Thus, the most common metastases we observe are in the peritoneal cavity – Omentum (fatty tissue that supports and covers organs in the lower abdomen), Ovaries, adnexa, and lymph nodes, and even spleen in some cases (Lisio et al., 2019).

Current treatment methods in HGSOC

Currently, the first line treatment for HGSOC involves primary debulking surgery (PDS) and platinum-based chemotherapy (Figure 1) (Nero et al., 2021b). However, size of the residual tumour mass after this cytoreductive surgery has shown to negatively correlate with patient prognosis (Polterauer et al., 2012). Given the challenges associated with achieving optimal tumour removal through PDS alone, neoadjuvant chemotherapy (NACT) followed by interval debulking surgery (IDS) has emerged as an alternative approach (Onda et al., 2008). The standard chemotherapeutic regimen for advanced HGSOC currently consists of a combination of carboplatin and paclitaxel. However, approximately 15% of patients develop resistance to this treatment regimen (Katsumata et al., 2013). Additionally, depending on the Homologous recombination deficient status of the patient, they are also prescribed with Poly (ADP-ribose) polymerase inhibitors (PARPi)(Rose et al., 2020).

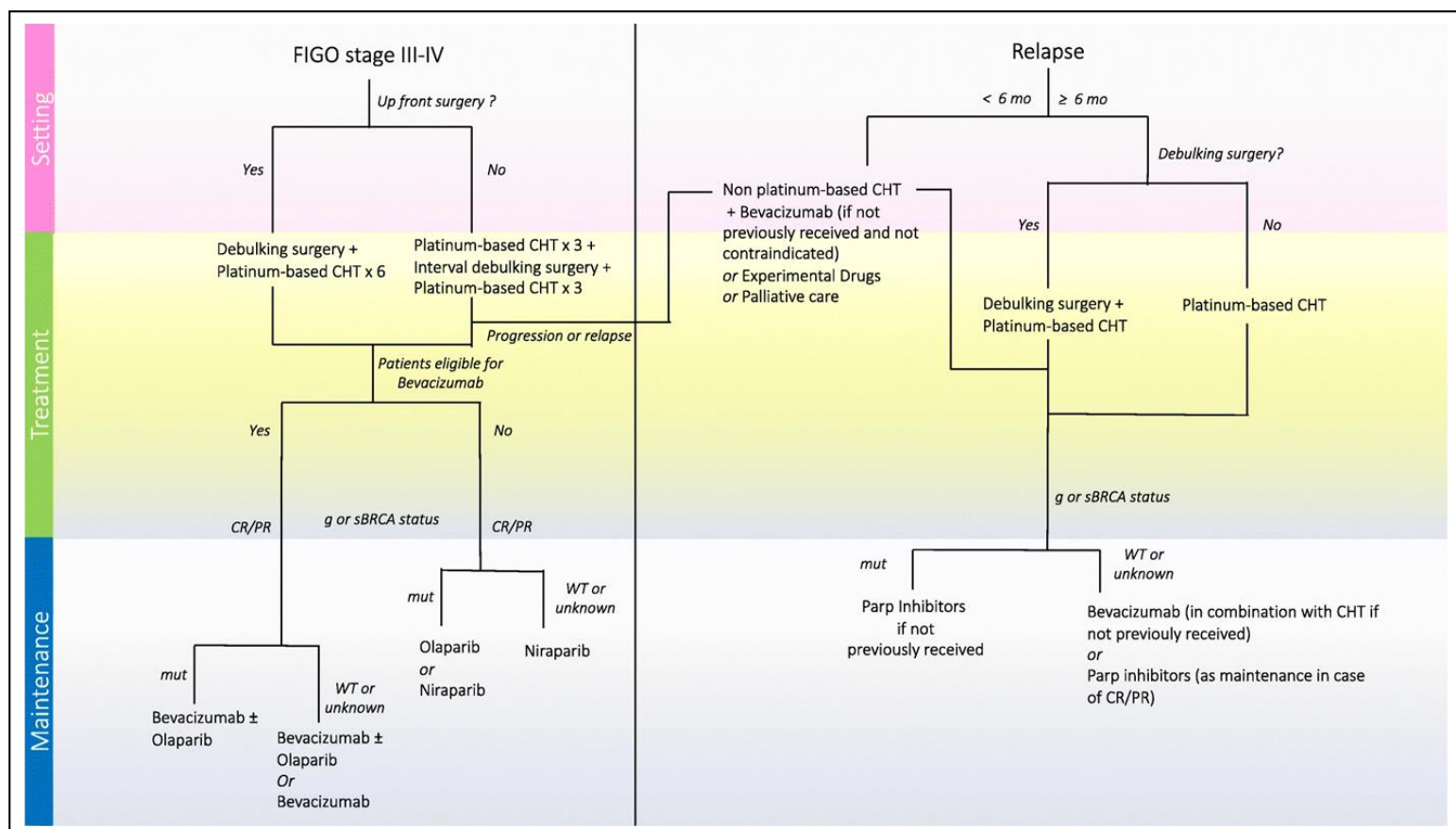


Figure 1: Current treatment plan for HGSOC patients (Nero et al., 2021b).

Despite significant advancements in therapeutics, the survival rate for high-grade serous ovarian cancer (HGSOC) has remained stagnant at around 45%-50% for several decades (Surveillance Research Program, 2021). This is mainly because of the high degree of heterogeneity found in the Tumour Microenvironment (TME), not

only across tumours but also within them. This attributes the malignancy to different immune evasion and resistance mechanisms, resulting in treatments succeeding in just a subset of the patient population (Vázquez-García et al., 2022) While approximately 80% of HGSOC patients initially respond to platinum-based chemotherapy, a significant portion—about 75%—eventually experience relapse (P.-E. Colombo et al., 2014). Moreover, the median progression-free survival in HGSOC patients is only 18 months, with a high likelihood of recurrence (Stewart et al., 2019).

Importance of DNA damage repair pathways in treatment

Recent research developments have identified a considerable amount of genomic heterogeneity, instability and mutations causing Homologous Recombination Deficiency (HRD), among others (Figure 2) (Cojocar et al., 2018). These mutations are major loss of function or epigenetic inactivation of the proteins BRCA1/2, which are integral in HR-mediated repair (P. E. Colombo et al., 2014). These tumour subtypes have been shown to have impaired response to DNA damage and increased sensitivity to drugs that target alternate DNA repair pathways/mechanisms, such as PARPi. One possible reason might be the synthetic lethality induced as result of 2 different DDR pathways getting perturbed/ inhibited (de Bono et al., 2020). Similarly, deficiency in the Mismatch Repair (MMR) pathway/ mechanism is associated with heightened sensitivity to PD-L1 (Programmed Death – Ligand 1) inhibitors (Morand et al., 2021).

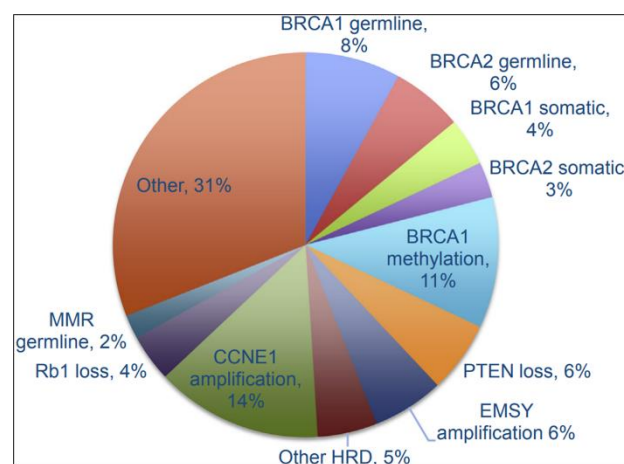


Figure 2: Mutations commonly seen in HGSOC patients. Most of these mutations are present in DNA damage response, repair, and cell cycle (Morand et al., 2021).

Short term Organoids have been used previously for functional profiling of DNA repair mechanisms and detecting vulnerabilities. They showed that, irrespective of DNA repair gene mutational status, a defect in homologous recombination (HR) increased

PARPi sensitivity and a defect in replication fork stability and protection was associated with ATR (Ataxia telangiectasia and Rad3 related) inhibitor sensitivity (Hill et al., 2018).

Recently, our lab had developed a method to characterize patients based on their allelic imbalances conferring them with increases susceptibility to HR targeted therapies. This method – ovaHRDscar, which scores the patient/ tumour based on allelic imbalances such as *BRCA1/2* mutations has also been adopted by the clinics for better and personalized treatment plans (Perez-Villatoro et al., 2022).

Immune microenvironment in HGSOc

Tumour immune microenvironment (TIME) composed of infiltrated immune cells, cytokines and chemokines acts as a crucial factor in the processes of cancer development, progression, and metastasis (Baci et al., 2020). Clinical effects of therapeutics are heavily dependent on these complex dynamics (Lei et al., 2020).

The immunophenotype of tumour microenvironment in HGSOc can be broadly classified into 3 different subtypes (Figure 3); immune cell inflamed (hot tumours) – which has immune cell infiltrates in tumour tissue and the surrounding stroma, immune excluded – where the immune cells are restricted to stroma and Immune desert (cold tumours) – which contain non inflamed immune cells (Chen & Mellman, 2017).

High-Grade Serous Ovarian Cancer (HGSOc) stands out among ovarian cancer subtypes for its significant infiltration of CD8+ T cells (Zhang et al., 2003). Moreover, the presence of CD8+ intraepithelial tumour-infiltrating lymphocytes (TILs) emerges as a positive prognostic indicator across HGSOc cases, irrespective of factors such as the extent of surgical cytoreduction, chemotherapy regimen, or the presence of germline *BRCA1* mutation (Goode et al., 2017).

Dendritic cells (DCs) capture, process and present non-host antigens to other immune cells (Théry & Amigorena, 2001). Antigen presented by DCs can be both exogenous (MHC class II molecules present antigens to CD4+ T cells) and/ or endogenous (MHC class I molecules present antigens to CD8+ T cells) (Dudek et al., 2013). The cytokine/ chemokine network is, in particular, involved in cancer related inflammation, angiogenesis, and immune cell infiltration (Kulbe et al., 2012). Interactions with antigen presenting cells (APCs) and T cells are one of the 3 requirements (presence of a cognate antigen and pro inflammatory signals being the other 2) for the appropriate

functional activation of exhausted CD8+ T cells (Mempel et al., 2004). These interactions are concordant with enhanced memory, effector function, survival, and proliferation in T cells (Duraiswamy et al., 2021).

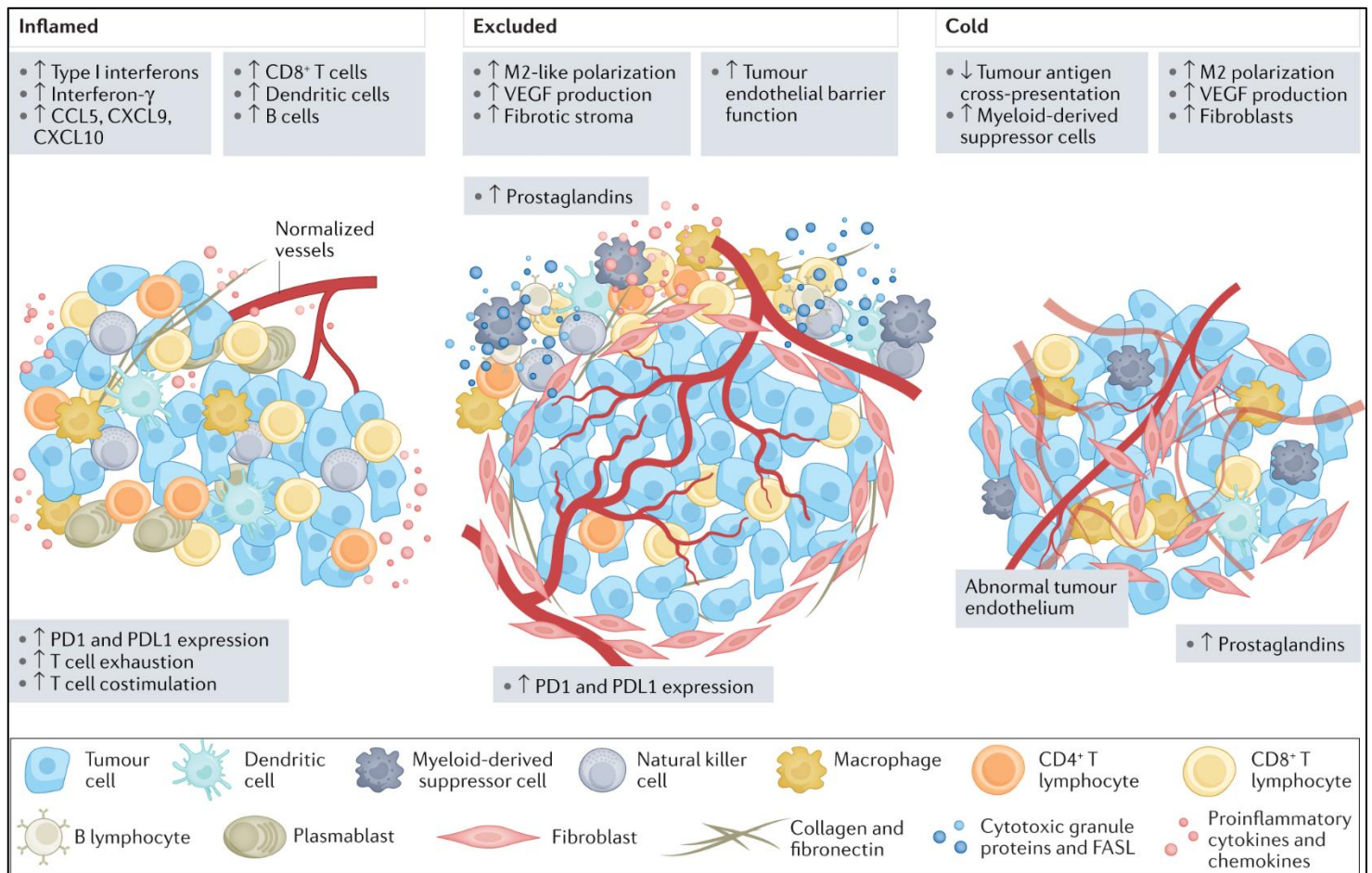


Figure 3: Immunophenotypes in HGSOC (Nero et al., 2021b).

Immunotherapy in Cancer Research and combining it with DNA damaging drugs

HGSOC patients are seen to be generally unresponsive to immunotherapies, especially towards anti PD1 antibody. This might be because of the low baseline expression of CD28 in a large portion of these tumours (Duraiswamy et al., 2021). Success of most immunotherapy regimens hinge upon pre-existing intratumoural immune cell inflammation. Thus, restoration of this inflammation is a crucial step in immunotherapy against cold or immune excluded tumours (Kandalaft et al., 2022). Presence and functional activation of DCs are essential for sustained anti-cancer responses (Duraiswamy et al., 2021). Different classes of drugs use different pathways for facilitating this.

PD-1/ PD-L1 (Programmed death/ programmed death ligand 1) axis is an important negative regulator for immune cell activity and is essential in the context of immune tolerance, autoimmunity, and immune cell exhaustion (Francisco et al., 2010). PD-L1 is majorly expressed in hematopoietic cells such as macrophages, T cells, B cells, dendritic cells, and mast cells. They are also expressed in some of the non-hematopoietic cells with their primary function being immune homeostasis (Sun et al., 2018). However, several tumour types, including HGSOc mimic this negative regulatory mechanism, expressing PD-L1 and essentially thwarting an immune response against them (Li et al., 2018). The binding of anti-PD1-antibodies to PD-1 in the T cells prevents this interaction, aiding in proper immune response. Inhibition of Autotaxin (ATX) is another mechanism which can be used to activate antigen presenting cells, mainly DCs. This happens due to the inhibition of Lysophosphatidic acid (LPA), which acts as a negative regulator of the functional activation and signaling in DCs and other innate immune cells (Emo et al., 2012). Majority of the LPA in our system is produced by the conversion of phospholipase A1 (PLA1) and phospholipase A2 (PLA2) family members converts phospholipids to lysophospholipids which is then converted to LPA by ATX(Aoki, 2004). Thus, ATX inhibits LPA production and removes the negative regulatory effects of the latter on DCs and other innate immune cells. DC: T cell co cultures were also seen to significantly increase the T cell proliferation and activation(Emo et al., 2012).

The rationale behind using DNA damaging drugs in combination with immunotherapy agents is that combination of low dose radiotherapy (DNA – damage inducing) with the latter was observed to induce inflammation and reduced metastatic solid tumour mass (Herrera et al., 2022). Furthermore, several pre-clinical work has now shown that other than the direct cytotoxic effects of these drugs, they alter the inflammatory response in the TME, promote immunogenic cell death and/ or stimulate neoantigen production which activates anti tumour activity in immune cells (Brown et al., 2018). PARPi has shown great synergistic effects with multiple immunotherapy regimens including anti-PD-1 antibodies(Konstantinopoulos et al., 2019) (Vikas et al., 2020).

Inhibition of PARP, a mainstream anti-cancer approach, has been demonstrated to selectively eliminate tumor cells while sparing normal ones (Sachdev et al., 2019). Members of the PARP family, such as PARP1 and PARP2, serve as DNA damage sensors and signal transducers. Inhibiting PARP disrupts the repair of single-strand

breaks (SSBs) (Schreiber et al., 1995). This effect is particularly pronounced in patients with HR deficiency, as the escalation of single-strand breaks to double-strand breaks (DSBs) remains unresolved (Saleh-Gohari et al., 2005). Though, only 40% of HRD patients have shown sensitivity to PARPi therapy (Audeh et al., 2010). Ovarian cancer patients who responded well against the combination of PARP inhibitor and an anti – PDL1 agent, had an exhausted TIL phenotype before the commencement of the treatment (Färkkilä et al., 2020). Another method is by inhibiting ATR, which is a DDR kinase. In most cancer cells, the G1 checkpoint is lost and there is an increased reliance in S and G2/ M checkpoints (Massagué, 2004). ATR is a pivotal in the S and G2/ M checkpoint signaling in the presence of ssDNA (Saldivar et al., 2017). As TP53 mutations (disruption of G1 checkpoint) are present in almost all HGSOC cancer tissue, it could render them more sensitive to ATR inhibition (Kwok et al., 2016).

The efficacy of combinations of DNA damaging drugs and immunotherapy drugs needs to be tested in their ability to kill tumour cells without adversely affecting the immune cells (and other host cells). There are no models which can recapitulate the patient specific tumour immune microenvironment.

Immunocompetent cultures as a model system and preliminary results

To recapitulate patient specific immune response, the lab has been focused on establishing a patient-derived immunocompetent model to test this in addition to studying the functional activation of the immune cells (CD8+ T cells, CD4+ T cells and CD11c+ cells).

The lab had previously found that growing HGSOC patient derived tumour cells in a patient-derived omentum gel matrix significantly improved the growth of HGSOC immunocompetent patient-derived cultures (iPDCs) compared to the conventional basement matrix. These iPDCs could maintain the tumour-derived lymphocytes and myeloid cells to a greater degree, while providing the tumour cells to grow in native-like environment. The iPDCs also showed inter-tumoral heterogeneity and tumour-specific drug responses (Ashwini S Nagaraj et al., 2024) in concordance with recent research findings (Nero et al., 2021b).

This model was used to test the efficacies of PARPi, ATRi and WEE1i (Wee1-like protein kinase inhibitor), which are DNA damage-inducing drugs; anti-PD-1 antibody,

which is an established immunotherapeutic drug; STING (Stimulator of interferon genes) agonist, ATXi and PERKi (Protein Kinase R (PKR)-like endoplasmic reticulum kinase), which are novel immunotherapeutic drugs.

Different concentrations of their monotherapies and combination therapies were tested in the iPDC model. The results showed promising results in monotherapy and combination therapies involving ATRi (Figure 4), especially the combination of ATRi and ATXi causing cancer cell death (Ashwini S Nagaraj et al., 2024). As this experimental set-up focused mainly on the effect of drugs on cancer cell death, we set out to investigate the effect of ATRi as a single agent or in combination with ATXi on the functional status of the T cells and dendritic cells. Using multi-parameter flow cytometry, we evaluate T cell activation using the markers IFN γ , granzyme B (GrzB), and Ki67, and for the dendritic cells, IFN γ , HLA-Dr and Ki67.

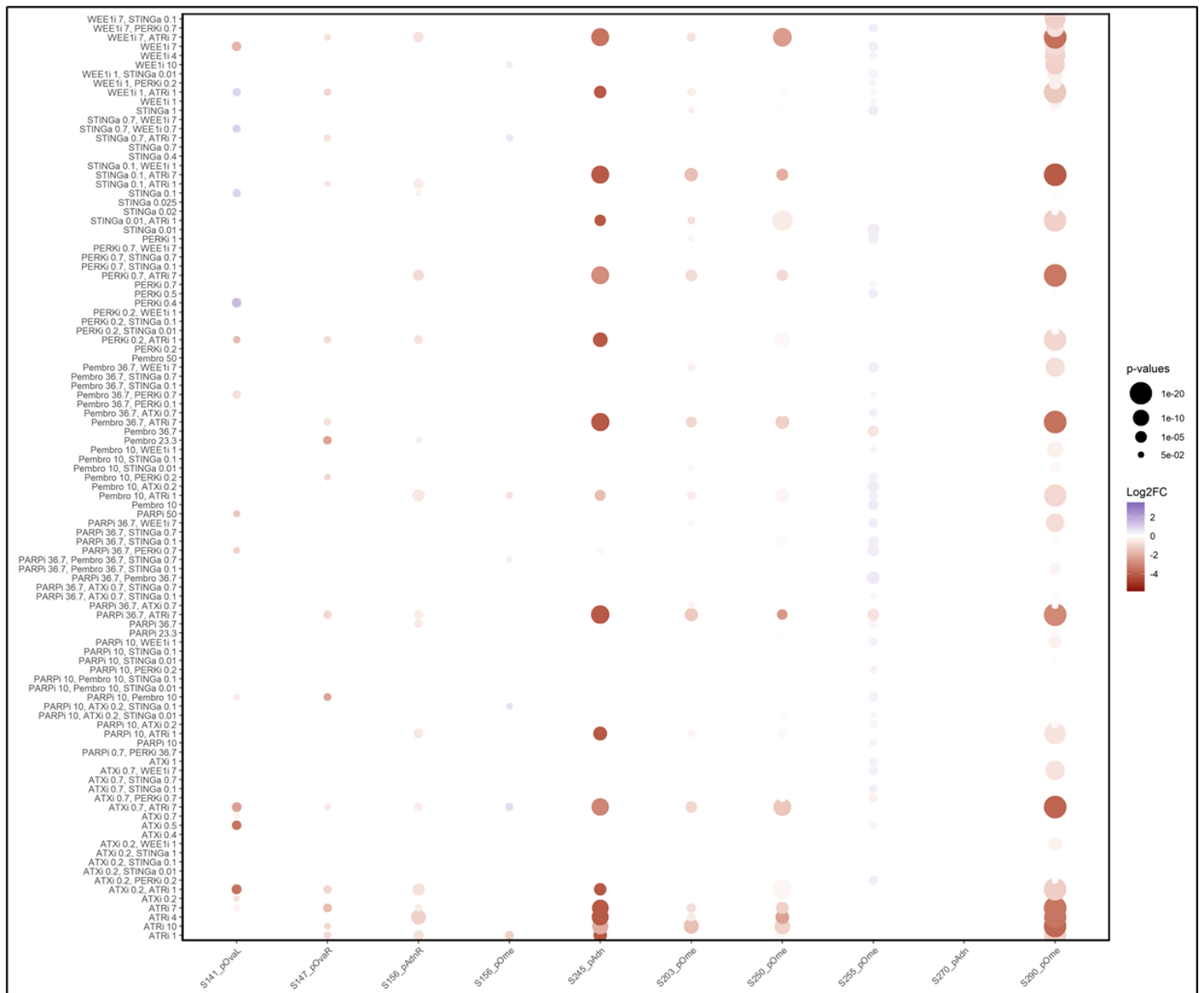


Figure 4: Monotherapies and combination therapies of different classes of drugs on HGSOc iPDcs. The dot plot shows the action of different concentration of monotherapies of Olaparib (PARPi), Pembrolizumab (anti PD-1 antibody), Berzosertib (ATRi), Ziritaxestat (ATXi), AMG PERK 44 (PERKi), GSK3859856 (STING agonist) and Adavosertib (WEE1i), and their different combinations. Each dot is a particular treatment in a particular sample. The log2FC shows the difference in the number of CK7+ (tumour) cells between control and each of the treatments. (unpublished data)

Project Idea

Due to the inherent heterogeneity of HGSOE tumours or any tumour in general, the use of combination drugs could possibly reduce the tumour mass to a greater extent when compared to monotherapies. Also, the majority of the pre-clinical drug treatment studies are primarily focused on cancer cell death, and the effect of single or combination therapies on immune cell abundance and functional states is poorly studied.

This thesis investigates the effects of single agent ATRi or ATXi and their combination treatment on T cells and DC functional states using GrzB, Ki-67, IFN γ and HLA-DR markers, as well as the cytotoxic effect of these treatments on cancer cells. Already established anti-cancer drugs such as Olaparib (PARPi) and Pembrolizumab (anti PD-1 antibody) were used for validation.

Objectives

1. To validate the action of drugs in patient derived immunocompetent cultures
 - To observe the change in immune cell proportion upon treatment with Olaparib and Pembrolizumab and their combination in the iPDOs
 - To check the immune cell (CD8+ T cell, CD4+ T cell and CD11c+ cell) functional activation (GrzB, Ki-67, IFN γ and HLA-DR) upon treatment with Olaparib and Pembrolizumab and their combination in the iPDOs
2. To check the effects of Berzosertib + Ziritaxestat and their combination in patient derived immunocompetent cultures
 - To observe the change in immune cell proportion upon treatment with different concentrations of Berzosertib and Ziritaxestat and their combination in the iPDOs
 - To check the immune cell (CD8+ T cell, CD4+ T cell and CD11c+ cell) functional activation (GrzB, Ki-67, IFN γ and HLA-DR) upon treatment with different concentrations of Berzosertib and Ziritaxestat and their combination in the iPDOs
 - To check the tumor and immune cell death upon treatment with different concentrations of Berzosertib and Ziritaxestat and their combination in the iPDOs

Materials

Name	Stock Concentration	Working Concentration	Company/ Catalogue
Advanced DMEM/F12			Thermo Scientific/ #12634-010
Primocin	50 mg/ml	100 µg/ml	Invivogen / #ANTPM1
NEAA	100x	1x	Gibco/ #11140035
Sodium Pyruvate	100x	1x	Gibco/ #11360-039
L-Glutamine	100x	1x	Gibco Life Technologies/ #35050-061
HEPES	100x	1x	Sigma Merk/ #H0887-100ML
N-Acetyl-Cysteine	100 mM	1 mM	Sigma/ #A9165-100G
Nicotinamide	100 mM	5 mM	Sigma/ #N0636-500G
Supplement B-27	50 x	1X	ThermoFischer/ #17504044
FGF-10	100 µg/mL	10 ng/mL	Peprotech/ #100-26
basic FGF (FGF4)	100 µg/mL	10 ng/mL	Peprotech/ #AF-100-18B
A-83-01	10 mM	0.5 µM	Sigma/ #SML0788-5MG
β-estradiol	10 mM	10 nM	Sigma/ #E2758-1G
Neuregulin-1 / Heregulin	6.6 µM / 50 ug/ mL	5 nM	Peprotech/ #100-03
EGF	100 µg/mL	5 ng/mL	Peprotech/ #AF-100-15
Hydrocortisone	1 mg/mL	500 ng/mL	Sigma/ #H0888
Y-27632 / ROCK inhibitor	5 mM	5 µM	AbMole Biosciences/ #M1817

Table 1: Reagents needed for base organoid media

Name	Stock Concentration	Working Concentration	Company/ Catalogue
IL2	66 X E6 IU/MI or 1mg/mL	500 IU/mL	Peprotech/ #200-02
IL15	10 µg/ml	10 ng/ml	Peprotech/ #200-15
IL7	10 µg/ml	10 ng/ml	Peprotech/ #200-07

Table 2: Interleukins needed for the complete organoid media

Name	Stock Concentration	Working Concentration	Company/ Catalogue
Ome-gel	17.7 mg/ml	2.5 mg/ml	
Aprotinin	10 mg/ml	33.3 µg/ml	Sigma-Aldrich/ #A6279
Thrombin	100 U	0.3 U	Sigma-Aldrich/ #T6884
Fibrinogen	25 µg/ml	0.5 µg/ml	Sigma-Aldrich/ #341578

Table 3: Omentum culture constituents

Name	Class of Drugs	Stock Concentration	Company/ Catalogue
Pembrolizumab	PARP inhibitor	5mg/ml	Selleckchem/ A2005
Ziritaxestat (GLPG1690)	ATX inhibitor	1mM	MedChemExpress/ HY-101772
Berzosertib (VE-822)	ATR inhibitor	10mM	Selleckchem/ S7102
Olaparib	Anti-PD1-Antibody	10mM	Selleckchem/ S1060

Table 4: Drugs used in the experiments

Fluorochrome	Antigen	Clone	Company/ Catalogue	Host	Dilution
FITC	CD56	MEM-188	Immunotools/ #21270563	Mouse	1:50
PE	CD14	18D11	Immunotools/ #21620144	Mouse	1:50
PE-CF594	CD4	ROA-T4	BD Biosciences™/ #562281	Mouse	1:50
PerCP-CY5.5	HLA-DR	G46-6	BD Pharmingen™/ #552764	Mouse	1:25
APC/Fire 75	CD326/ EpCam	9C4	Biolegend/ #324233	Mouse	1:50
BV421	CD45	HI30	BD Biosciences™/ #563879	Mouse	1:200
BV510	DCM		Invitrogen™/ #L34965	Mouse	1:200

BV510 (for compensation)	CD16	3G8	BD Biosciences/ #563829	Mouse	
BV605	CD8	SK1	BD Biosciences™/ #564116	Mouse	1:50
BV711	CD11c	B-ly6	BD Horizon™/ #563130	Mouse	1:50
BV786	CD3	SK7	BD Horizon™/ 563800	Mouse	1:50

Table 5: List of fluorochrome-tagged antibodies for surface antigens

Fluorochrome	Antigen	Clone	Company/ Catalogue	Host	Dilution
PE-CY7	Ki-67	B56	BD Pharmingen™/ 561283	Mouse	1:50
APC	GrzB	GB11	Invitrogen/ GRB05	Mouse	1:50
APC/Fire 750	IFN γ	B27	BD Pharmingen™/ 557995	Mouse	1:50

Table 6: List of fluorochrome-tagged antibodies for intracellular antigens

Channel	Name	Company/ Catalogue	Dilution
555	Anti-CK7	Abcam/ #EPR17078	1:250
647	Anti-CD45	BioLegend/ #304018	1:150
350	Hoechst	ThermoFisher/ #H3570	1:8000
488	Live-or-Dye Fixable viability dye	Biotium/ #32004A	

Table 7: IF antibodies, their standardized concentrations

Name	Company/ Catalogue
Advanced DMEM/F12	ThermoFisher/ #12634010
DMEM/F12 with L-Glutamine	Thermo Fisher/ #1320033

Table 8: List of medias used in the experiments

Name	Company/ Catalogue
CS&T Research Beads	BD Biosciences/ #655051
Fixable Live-or-Dye™	BD biosciences/ #552843
RQ1-RNase free DNase	Promega/ #M610A
RBC lysis buffer	Sigma Aldrich/ # 11814389001
Stem cell banker	Amsbio/ #11890F
BD™ CompBeads Anti-Mouse Ig, κ/Negative Control Compensation Particles Set	BD Biosciences/ #552843
BSA	
EDTA	
FBS	
Dispase	Sigma-Aldrich/ #D4693

Glutamax	Thermo Fisher/ # 35050061
1X DPBS	Thermo Fisher/ #14190094

Table 9: Other solutions used in the experiments

Name	Company/ Catalogue
70µm cell strainer	Thermo Fisher/ #22363548
15ml Falcon tubes	Greiner Bio-One/ #3913477
50 ml falcon tubes	Greiner Bio-One/ #525-0384
5ml pipettes	Greiner Bio-One/ #6121013
10ml pipettes	Greiner Bio-One/ #6121015
25ml pipettes	Greiner Bio-One/ #6121017
10 cm dish	Greiner Bio-One/ #391-3236
2ml Cryotubes	Greiner Bio-One/ #4790086
Cell Freezing box	Biocision/ #BCS-136
Cell Counting Slides	Logos Biosystems/ #L12001
Stainless steel microscopy scissors	Thermo Fisher/ #10065090/4070
Sterile disposable scalpels	Thermo Fisher/ #11798343/0501
Stainless steel forceps	Thermo Fisher/ #10169920/1002

Table 10: Miscellaneous items used in the experiments

Buffers, reconstitutions and preparations

Base tissue dissociation media preparation

5 ml of 100X Glutamax, 5 ml of 1M HEPES and 5 ml of Pen Strep was added to 500 ml of DMEM/F12. The base tissue dissociation media is prepared beforehand and is stored in 4°C.

Dispase preparation

50U/ml stock of dispase was prepared by dissolving the powder in a buffer containing 5mM CaAc and 10mM NaAc (pH 7.5) using a filter tip of 0.22 µM. Aliquots were stored in 4°C until use.

Dissociation final solution preparation

Final dissociation solution was prepared by mixing the base tissue dissociation media with prepared dispase solution and RQ1-RNase free DNase in the volume ratio 97:2:1.

Recombinant Human Neuregulin β reconstitution

50 ug/ ml stock is prepared by dissolving 100 µg in 2 ml of sterile filtered (0.22 µm) 0.1% (w/v) BSA in DPBS (without Ca²⁺ and Mg²⁺). Aliquots were stored in -80°C until use.

rhEGF reconstitution

1 mg of powdered rhEGF was dissolved in 10 ml of 0.1% (w/v) sterile filtered (0.22 µm) BSA in DPBS (without Ca²⁺ and Mg²⁺). Aliquots were stored in -80°C until use.

rh FGF-10 reconstitution

25 ug of powdered rh FGF-10 was dissolved in 250 µl of 0.1% (w/v) sterile filtered (0.22 µm) BSA in DPBS (without Ca²⁺ and Mg²⁺). Aliquots were stored in -80°C until use.

Rh FGF- Basic reconstitution

50 µg of powdered rh FGF- basic was dissolved in 500 µl of 0.1% (w/v) sterile filtered (0.22 µm) BSA in DPBS (without Ca²⁺ and Mg²⁺). Aliquots were stored in -80°C until use.

Interleukin-2 reconstitution

1mg of IL-2 powder was dissolved in 1 ml of 0.1% (w/v) sterile filtered (0.22 µm) BSA in DPBS (without Ca²⁺ and Mg²⁺). Aliquots were stored in -80°C until use.

Interleukin-7 reconstitution

10 µg of IL-2 powder was dissolved in 1 ml of 0.1% (w/v) sterile filtered (0.22 µm) BSA in DPBS (without Ca²⁺ and Mg²⁺). Aliquots were stored in -80°C until use.

Interleukin-15 reconstitution

10 µg of IL-2 powder was dissolved in 1 ml of 0.1% (w/v) sterile filtered (0.22 µm) BSA in DPBS (without Ca²⁺ and Mg²⁺). Aliquots were stored in -80°C until use.

N-Acetyl-L-cysteine reconstitution

1.6 g of N-Acetyl-L-Cysteine powder was dissolved in 100ml of milli-Q. It was sterile filtered (0.22 µm) and stored in 4°C until use.

Thrombin from Human Plasma reconstitution

100 units of Thrombin was diluted in 1 ml of 0.1% (w/v) sterile filtered (0.22 µm) BSA in sterile PBS. Aliquots were stored in -80°C until use.

Fibrinogen preparation

Powdered fibrinogen was warmed to 37 °C. 10 ml of warm sterile Milli-Q was added to it. As the fibrinogen solution gets viscous while pipetting, it was warmed in the water bath multiple times. After dissolving, 10 ml of warm sterile milli-Q is again added to the solution.

Aprotinin reconstitution

25 mg of Aprotinin powder was dissolved in 2.5 ml of milli-Q. Aliquots were stored in -20°C until use.

Drug Dilutions

The drugs were diluted (Table X) on the day they were added to the cultures.

Compound	Stock Concentration	Working Concentration	7X concentration	Volume of drug per 600 µL	Volume of the media (in µL)	Samples treated
DMSO (Control)	100%	0.2%	1.4%	16.8 µL	583.2	S321, S333, S263
Berzosertib/VE-822 (ATRI)	0.1 mM	20 nM	140 nM	0.84 µL	599.16	S321, S333, S263
Berzosertib	See above	100 nM	700 nM	4.2 µL	595.8	S321, S333, S263
Berzosertib	See above	1 µM	7 µM	42 µL	558	S321, S333, S263
Ziritaxestat/GLPG1690 (ATXi)	0.1 mM	0.13 µM	0.65 µM	3.9 µL	596.1	S321, S333
Ziritaxestat	See above	0.2 µM	1.4 µM	8.4 µL	591.6	S321, S333, S263
Ziritaxestat	See above	0.7 µM	4.9 µM	29.4 µL	570.6	S321, S333, S263

Berzosertib + Ziritaxestat -	See above	20 nM + 0.13 μ M	140 nM + 0.65 μ M	0.84 μ L + 3.9 μ L	595.3	S321
Berzosertib + Ziritaxestat	See above	20 nM + 0.2 μ M	140 nM + 1.4 μ M	0.84 μ L + 8.4 μ L	590.8	S333, S263
Berzosertib + Ziritaxestat	See above	100 nM + 0.2 μ M	700nM +1.4 μ M	4.2 μ L + 8.4 μ L	587.4	S321, S333, S263
Berzosertib + Ziritaxestat	See above	1 μ M + 0.2 μ M	7 μ M + 1.4 μ M	42 μ L + 8.4 μ L	546.6	S321, S333
Olaparib (PARPi)	10mM	20 μ M	140 μ M	8.4 μ L	591.6	S321, S333, S263
Pembrolizumab (anti-PD1-antibody)	5mg/ml	10 μ g/ml	70 μ g/ml	8.4 μ L	591.6	S321, S333, S263
Olaparib + Pembrolizumab	See above	20 μ M + 10 μ g/ ml	140 μ M + 70 μ g/ ml	7 μ L + 7 μ L	583.2	S321, S333, S263

Table 11: All the drug dilutions and combinations used for experiments.

FACS buffer preparation (50 ml)

1ml of FBS was added to 48.8 ml of 1X PBS in sterile conditions. 200 ml of 0.5M EDTA was sterile filtered (0.22 μ m) to this mixture.

1X Permeabilisation buffer preparation

5ml of 10X permeabilisation buffer was added to 45 ml of milli-Q to make 1X permeabilisation buffer. It was stored in 4°C until use.

Blocking buffer Preparation (Immunofluorescence)

0.45g of Bovine Serum Albumin was added to 15 ml of 1X DPBS. The container was placed in a magnetic stirrer for 10-30 minutes. Post dissolving, 45 μ L of Triton X-100 was added and the container was left in the magnetic stirrer for 15 more minutes.

Methods

Sample collection, preparation, and storage

HGSOC tissue samples were collected with the approval of the ethical board of the Women's Hospital Helsinki University Hospital. Depending on the size, the samples were kept in a 10cm or 15cm plate for primary processing. Soft tissues, membranes, and large blood vessels were removed (Figure 5). Six small pieces from the tissue (preferably adjacent) were cut, two each for DNA, RNA, and protein isolation. The remaining tumour tissue is brought back to the lab for cell culture. The tumour pieces were then minced using a scalpel and /or scissors. The minced tissue is then transferred to a 50ml falcon tube containing 9700 μ L DMEM/F12 with HEPES + Penstrep and glutamax + 200 μ L of 50 U/ml of dispase (50U/ml) stock + 100 μ L RNase free DNase1. The sealed falcon is incubated at 37°C in a rotating incubator for 30 minutes. Contents of the 50 ml falcon were strained into another 50 ml falcon using a 70 μ L cell strainer. The strainer was pre-wet before (1ml) and after (5ml) straining with DMEM/F12. The sample was centrifuged for 10 minutes at 1000 rpm at 4°C. The supernatant was removed into 2% Virkon. The pellet was resuspended in 2mL-4mL RBC lysis buffer (depending on the size) and incubated for 5 minutes at room temperature. 10ml – 20ml of DMEM/F12 (10 ml of DMEM/F12 for 2 ml of lysis buffer) was added to the sample. The sample was centrifuged for 10 minutes at 1000 rpm at 4°C. The pellet was resuspended in 1ml-5ml of cold DMEM/F12 (depending on the pellet size). Viability of the sample was checked using 1:1 mixture of the cell suspension and Trypan blue in the LUNA cell counting chamber (20 μ L on each side). The remaining cells (after the required amount is taken for culture set up) were suspended in 2ml-5ml (depending on cell count) of stem cell banker. 1ml was aliquoted to each cryotube for storage at -80°C.

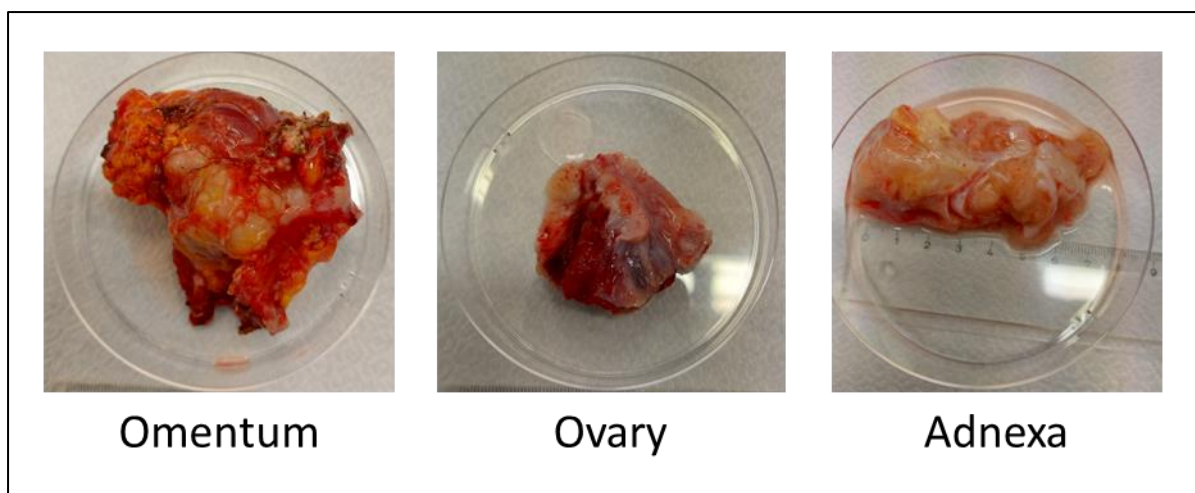


Figure 5: Tissue samples before the commencement of processing.

Organoid Culture (48 and 384 well plates)

Media preparation

Organoid media is prepared in a 2-step process. The base medium containing growth factors and supplements was prepared beforehand (Table 1). On the day of culturing, additional supplements supporting immune cell growth were added to the base medium (Table 2). (The composition of the media has been removed from the report submitted to the institute).

Organoid culture preparation and administration of drugs

Dissociated cells are resuspended in the appropriate amount of the prepared media. Omentum gel (prepared from tumour-free omentum of up to 5 patients), Aprotinin, Thrombin and Fibrinogen (Table 3) are added to the dissociated cells and plated as droplets for flow cytometry (48 well plate) or viability (96 well plate) analyses. The droplets are allowed to solidify for 60 minutes at 37°C cell culture incubator, followed by addition of 300 μ L of the culture medium (48-well plate) and 150 μ L for 96 well plate. 7X concentrated drugs are prepared (Table 11) and 50ul /25 ul per 48 well or 96 well are added and the plates were transferred back to 37°C incubator for 3 days.

Organoid dissociation

At the end of the drug treatment (3 days post-treatment), supernatant from each condition was collected in an Eppendorf. The remaining media was aspirated without disturbing the organoid culture. Dissociation media with 1U/ml dispase in DMEM-F12 dissociation media (same as the one used in patient tissue dissociation) was prepared.

300 μL of the solution was added per well and incubated at 37°C for 30 minutes. The matrix was detached and transferred to a 15 ml falcon. Falcons were centrifuged for 6 minutes at 400 rcf at 4°C . Supernatant was discarded, and 900 μL of FACS staining buffer was added per condition. Contents of the falcon were then transferred into the corresponding Eppendorf.

Flow Cytometry

Flow cytometry was done on the day of culturing (d0) and again on a subsequent day (d3/d4/d5) to see the effect of the drugs on the immune and tumour cell population.

Antibody staining

The surface antibody mix is prepared in 40.5 μL of brilliant stain buffer per sample. Antibodies (Table 5) are sequentially added to the Brilliant stain buffer (for a total volume of 50 μL) (The Dead cell marker (DCM) is added last as it is not an antibody and is found detrimental to the antibodies).

1×10^6 cells are aliquoted in an Eppendorf with 900 μL FACS staining buffer and is centrifuged for 6 minutes at 400 rcf at 4°C . Supernatant is discarded and cell pellet is resuspended in 48 μL of the antibody mix per sample and kept for incubation for 30 minutes at 4°C in dark. 900 μL FACS staining buffer was added to each sample and centrifuged it for 6 minutes at 400 rcf at 4°C . Supernatant was discarded and 200 μL of IC fixation buffer was added and incubated for 40 minutes at 4°C in dark. 1 ml of 1X permeabilisation buffer (in PBS) was added and incubated for 5 minutes at 4°C in dark. Supernatant was discarded post-centrifuge. The cell were washed with 1X permeabilisation buffer and centrifuged for 6 minutes at 400 rcf at 4°C . Supernatant was discarded and 900 μL of FACS buffer was added and kept for incubation at 4°C in dark for O/N. Intracellular antibody mix is prepared in 47 μL of brilliant stain buffer. Antibodies (Table 6) are sequentially added to the Brilliant stain buffer (for a total volume of 50 μL).

Post O/N incubation, the pellet is resuspended in the 48 μL prepared antibody mix and incubated for 30 minutes at 4°C in dark. Post-incubation it is washed with 1 ml of 1X permeabilisation buffer and centrifuged for 6 minutes at 400 rcf at 4°C . Supernatant was discarded and the pellet was resuspended in 250 μL FACS staining buffer. Sample

was shifted to a 5 ml falcon with a cell strainer cap (#352235). Samples must be kept in a cold and dark environment until running the flow.

Single colour compensations

1 drop of BD CompBeads Anti-Mouse Ig (#51-90-9001229) was added for every tube in a 5 ml polystyrene round-bottom falcon tube (#352052). 1 drop of BD CompBeads Negative Control (#51-90-9001291) and BD CompBeads Anti-Mouse Ig each was added for the negative control. 1 μ L of single fluorochrome-conjugated antibodies was added to the corresponding 5 ml falcon and incubate for 30 minutes at 4°C in the dark. Since DCM used was not an antibody, CD16 – BV510 conjugate was used for calculating the compensation of the channel. 250 μ L of FACS staining buffer was added to each tube before running the samples. PMT voltages were changed as required using the compensation.

Immunofluorescence (384 well plates)

Live/dye Staining

Media (along with drugs/ drug combinations) from the 384 wells were removed and washed with 70 μ L of 1X PBS. 20 μ L Fixable Live-or-dye™ stain diluted 1:1000 in 1X PBS was added to each of the well. The plates were incubated for 30 minutes at RT in dark. The cells were then fixed using 50 μ L 4% paraformaldehyde for 40 minutes in dark. Cells were washed with 70 μ L of 1X PBS 3 times. Post washing, 200 μ L of 1X PBS was left per well, the plate was sealed using parafilm and covered with tin foil. (This plate can be stored in 4°C for a few days.)

Antibody cocktail preparation

The antibodies were prepared just before staining. They were diluted in the prepared blocking buffer in specific dilutions (Table 7).

Antibody Staining and imaging

Media was removed from the 4% paraformaldehyde fixed plates. 30 μ L of blocking buffer was added to each well and was incubated in RT at dark for 60 minutes. Post incubation, the blocking buffer was removed from each wells and 15 μ L of prepared antibody cocktail was added to each well. The plates were incubated at 4°C O/N. Post incubation, each well was washed 70 μ L of 1X PBS 4 times. The imaging was done on OperaPhenix scanner.

Data Analysis

FlowJO

Flow Cytometry results were first analysed using FlowJO software. The compensations were changed to minimise leaking. From each of the samples, cells were selected (Forward Scatter Area V/S Side Scatter Area) from the total events. From this, single cells (Forward Scatter Area V/S Forward Scatter Height), Live cells (DCM V/S Side Scatter Area) and EpCam negative (EpCam V/S Side Scatter Area) were subsequently selected. Mean intensities of EpCam negative (non-tumour) cells for each marker were then exported as CSVs.

CYTO

The exported CSVs were then uploaded to CYTO (Casado et al., 2021). Data normalisation was done using the Z score. EpCam negative (non-tumour) cell were then clustered using FlowSOM clustering method into 25 different clusters using the immune cell type markers (CD45, CD3, CD8, CD4, CD14, CD11c, CD56) and the remaining markers (GrzB, IFN γ , Ki-67 and HLA-DR) were kept for visualisation (Figure 6). These clusters were then annotated manually into biologically relevant immune cell type (CD8+ T cells, CD4+ T cells, Other T cell types, Monocytes, Dendritic cells, Monocyte – derived dendritic cells, etc) by checking the expression levels of the different cell type markers (Figure 7).

Proportion bar plots were drawn using this annotated clusters per treatment per sample to identify the different immune cell types per treatment per sample. The expression levels of IFN γ , Ki-67 and HLA-DR were used to assess the functional activity of the CD11c+ cells, and the expression levels of GrzB, IFN γ and Ki-67 were used to assess the functional activity of the CD8+ T cells and CD4+ T cells. Heatmaps showing log₂ fold change of each functional marker per immune cell type per treatment was then plotted.

The screenshot displays the CYTO software interface with the following settings:

- Input data:**
 - Markers for clustering: CD11c, CD14, CD3, CD4, CD45, CD56, CD8, DCM, Epcam, FSCA, FSCH, FSCW, GrzB, HLADr, IFNg, Ki67, SSCA.
 - Markers for visualization: CD11c, CD14, CD3, CD4, CD45, CD56, CD8, DCM, Epcam, FSCA, FSCH, FSCW, GrzB, HLADr, IFNg, Ki67, SSCA.
- Data processing:**
 - Downsample before analysis? Yes No
 - Downsample from [redacted] to 10000 cells
 - Downsample method: random
 - Data transformation: none
 - Sample normalization: z-score
- Data analysis:**
 - Clustering method: FlowSOM
 - Number of clusters: 25
 - 2-dimensional embedding methods:
 - Downsample further before data embedding? Yes No
 - Down to 10000 cells
 - tSNE: Perplexity: 20, Theta: 0.03
 - UMAP: Min dist: 0.1, Number of k-Nearest Neighbors: 50

Figure 6: Settings used in CYTO to run each of the sample

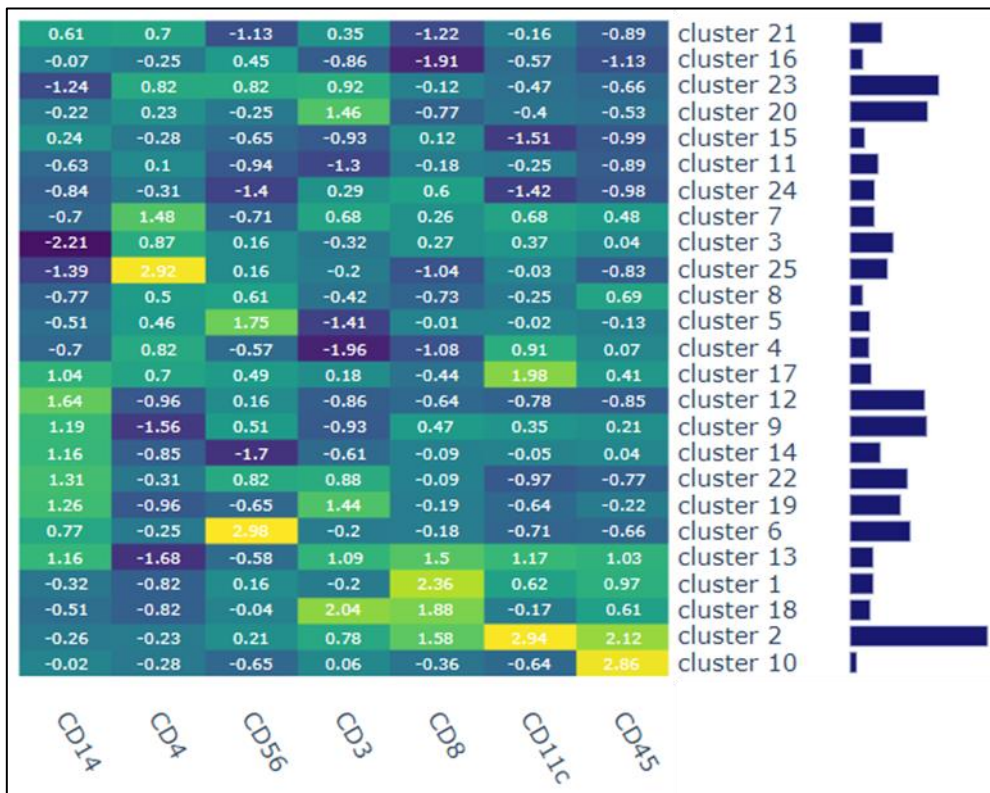


Figure 7: Example showing Z scores of each immune cell marker per cluster

Cell Profiler

After the Immunofluorescence images were flattened, they were segmented into different cell types using a Cell profiler pipeline. The flattened images were first split into large (tumour) cells and small (immune) cells based on their nuclei/cell size. A threshold value of 2500 was used to differentiate the two cell types from each other for all 3 samples.

The segmented images had intensity values for CK7 (tumour cells) and CD45 (immune cells) expression. These intensity values were manually analysed to find an optimal threshold which can segregate tumour cells and immune cells from each other. Intensity values from DCM were used to differentiate between the dead and alive cells within the tumour cell and immune cell cohort. Heatmaps were plotted using these threshold values to calculate the log2 fold change in tumour and immune cell death between control and each of the treatments.

Results

Tumour tissue samples from 4 out of 14 patients were suitable for culturing in omentum gel

The samples processed in this thesis were derived from Omentum (n=8), Adnexa (n=4), Ovaries (n=1) and spleen (n=1). The blood clots, cauterised tissue, and the associated tissues were removed from these samples and stored in Hanks' Balanced Salt Solution (HBSS) until processing. Post-dispase digestion and RBC lysis, the cell count (Table 12) was calculated to decide on further experiments.

The size of omental samples was generally larger than samples from other regions. They also had distinct solid tumour portions, which could be easily understood during the mincing of the sample. More cartilage-like tissues, which had little semblance to the tumour tissue, were observed in both ovarian and adnexa samples. Ovarian samples also had capsule-like structures, which made mincing the tissue harder. Subsequent experiments were done on samples that were clearly diagnosed as HGSOc, had sufficient cells, and formed clumps. The samples taken for further experiments – S321, S333, S263 were diagnosed as stage IVB High Grade Serous Carcinoma and were both BRCA wild type. Sample S321 had an HRD score greater than 50, indicating a Homologous Recombination Deficient genotype, while sample S333 had an HRD score less than 50, indicating a Homologous Recombination Proficient genotype. (The HRD score of S263 is yet not available.)

Sample ID	Site	Average cells per ml (in 10 ⁶)	Total cell number (in 10 ⁶)	Viability (in %)	Included for experiments	Reason for not being part of the study
S314_pOme	Omentum	4.96	9.92	31.8	No	Diagnosis not clear
S315_pOme	Omentum	1.14	1.14	27.7	No	Insufficient number of cells

S321_pOme	Omentum	11.5	57.5	76.5	Yes	Used for study
S330_pOva R	Right Ovary	2.85	5.70	58	No	Insufficient number of cells
S316_pOme	Omentum	9.32	9.32	60.4	No	Insufficient number of cells
S337_pOme	Omentum	1.8	1.8	50.25	No	Insufficient number of cells
S333_pOme	Omentum	10.2	51	76.5	Yes	Used for study
S331_pAdnL	Left Adnexa	5.3	5.3	70.1	No	Endometrioid carcinoma
S357_pAdn R	Right Adnexa	3.5	17.5	88.5	No	Clumps were not formed
S334_pOme	Omentum	0.9	0.9	57	No	Insufficient number of cells
S366_rSpl	Spleen	1.1	5.5	32	No	Insufficient number of cells
S371_pAdnL	Left Adnexa	1.2	3.6	86	No	Insufficient number of cells
S376_pAdnL	Left Adnexa	1.46	1.46	27.6	No	Insufficient number of cells
S263_pOme	Omentum	7	35	62.2	Yes	Used for Study

Table 12: Samples collected and processed with Sample ID, site of origin, cells per ml, total number of cells

Immunocompetent cultures were established successfully from 3 patient-derived tumours

The samples diagnosed as High Grade Serous Ovarian Cancer and with a sufficient number of cells (>10 million) were then used for immunocompetent culturing. The complete organoid media was made on day 0 (start of the culture). 4000 μL of omentum gel mix was prepared for 48 well plates - 78 wells (13 treatment conditions * 6 replicates) and 384 well plates – 54 (13 conditions * 4 replicates). 45 μL and 6 μL of omentum gel cultures were added as droplets to the wells, for 48 well and 384 well plates respectively, and were let to solidify for 60 minutes in the incubator at 37°C. Post incubation, we added 300 μl and 25 μl of media in each well, respectively, for 48 well and 384 well plates. The cells were allowed to settle in the 37°C incubator until next day, where the drugs were added. The cells were cultured for 72 hours post-drug treatment and harvested for flow cytometry.

Cultures were made with 4 different samples – 1 adnexa and 3 omental. Successful cultures were only established from the omental samples. Omentum samples were observed to have more clumps than the samples obtained from other areas and were thus deemed better for the drug treatment experiment. The clumps in the Omentum samples grew in size during the period of experiments, too (especially the control wells) (Figure 8). The adnexa sample processed during the span of the project mostly had single cells and minimal clumps. It was thus deemed unsuitable for the drug treatment experiments.

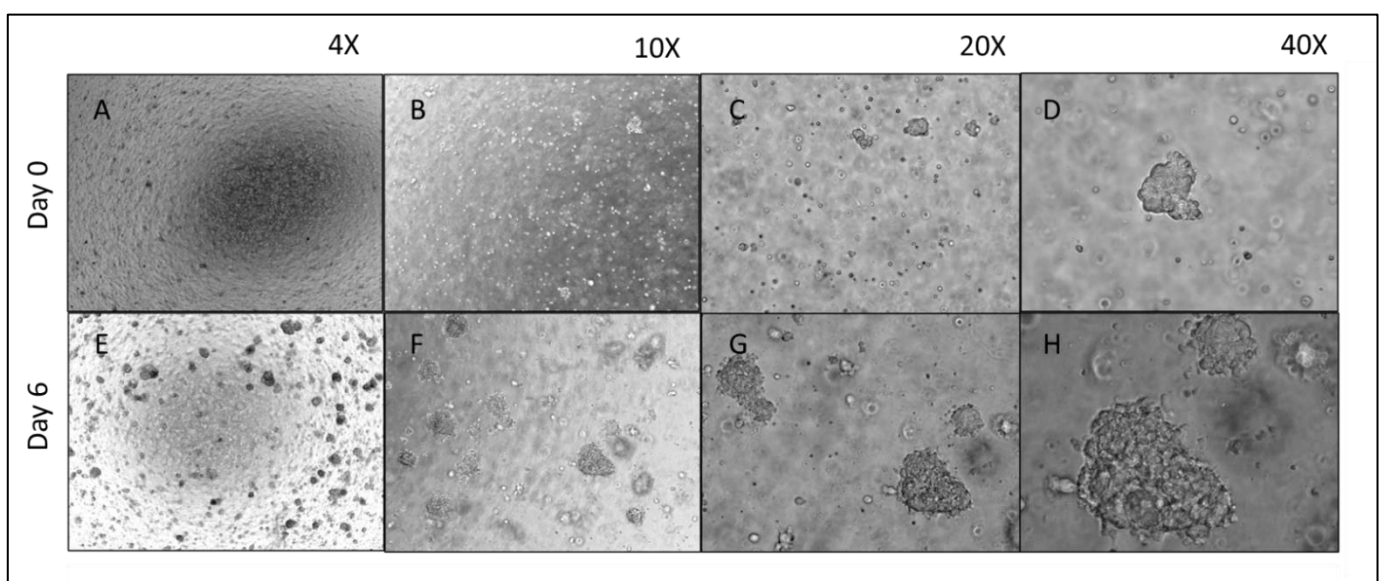


Figure 8: Immunocompetent cultures derived from Omental sample. Microscopy images of immunocompetent cultures on day 0 – **A)** 4X **B)** 10X **C)** 20X **D)** 40X and day 6 – **E)** 4X **F)** 10X **G)** 20X **H)** 40X

The immune cell population in the tumour tissue was recapitulated in the patient-derived immunocompetent cultures

The samples S321_pOme, S333_pOme and S263_pOme were used for further experiments as they had a clear HGSOE diagnosis, showed sufficient cells, and formed clumps. They were cultured in Omgel in 48 (for flow cytometry) and 384 well plates (for immunofluorescence (IF)). Flow cytometry analysis of these samples was done on the tumour-dissociated cells (day 0) to determine the immune cell composition of the tumour tissue. The cultures in the 48 well plates were dissociated 3 days post-treatment (day 4), followed by flow cytometry. EpCam negative cells (non-tumour cells) were exported from FlowJO and further analysed using CYTO. In CYTO, EpCam negative cells were clustered into 25 clusters using FlowSOM depending on the cell markers (CD45, CD3, CD56, CD11c, CD14, CD8, CD4). Based on the Z-score, these clusters were manually annotated into different cell types (Dendritic cells, Helper T cells, Macrophages, Cytotoxic T cells and undefined). The cell proportion per treatment was obtained from annotated clusters.

The immune cell composition of each sample was unique. It was a mixture of Dendritic cells (CD11c+), Monocytes (CD14+), Helper T cells (CD4+), Cytotoxic T cells (CD8+) and NK cells (CD56+). The immune cell composition in all 3 samples were recapitulated in the day 3 cultures (Figure 9). All the immune cells in the tissue sample were seen in the cultures, though with altered proportions. The proportion of myeloid cells (Dendritic cells and monocytes) increased in all 3 cultures. Lymphoid cell proportion in the samples S321 and S263 were reduced substantially compared to the d0 control. In the sample S333, the CD8+ T cell proportion showed negligible change, while the CD4+ T cell proportion markedly decreased.

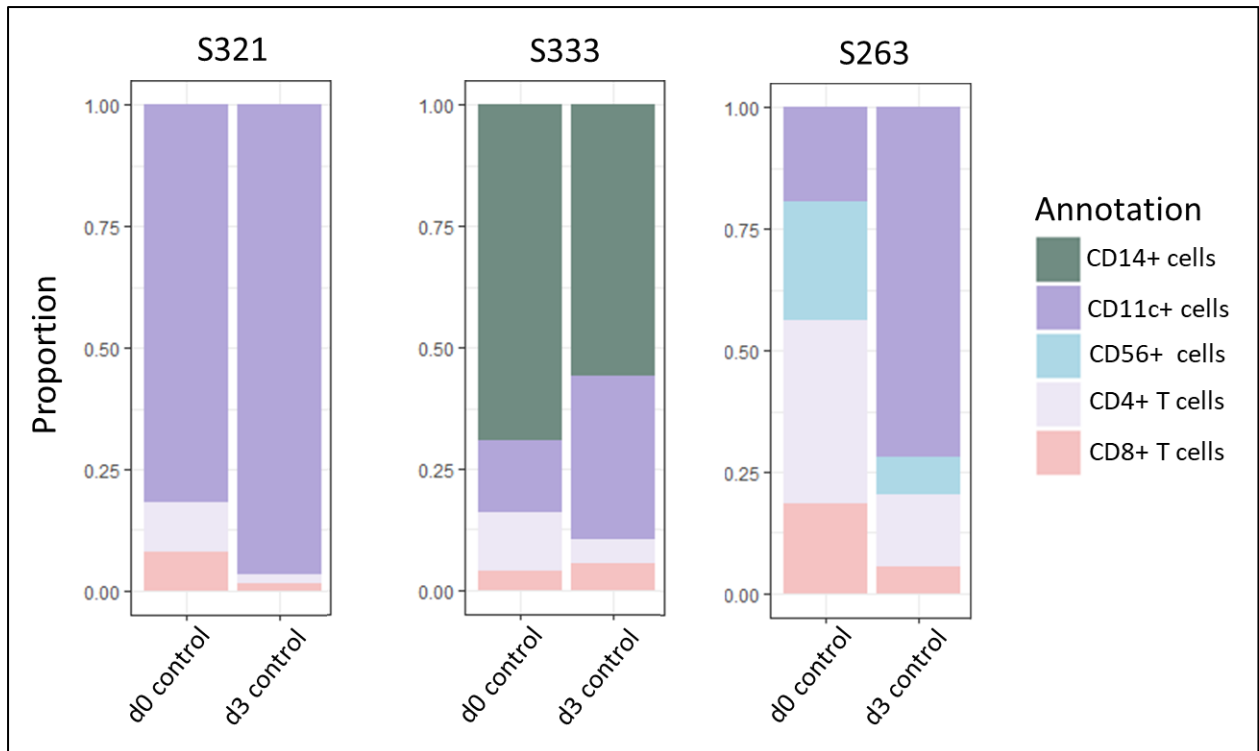


Figure 9: Immune cell proportion in the tumour tissue (day 0) and patient-derived immunocompetent cultures (day 3) from samples S321, S333 and S263. Each bar plot - S321, S333 and S263 shows the immune cell proportion obtained from flow cytometry on the day of tissue processing and the end of omentum gel culturing (post 72 hours). Proportions were obtained by clustering EpCam negative (non-tumour) cells using FlowSOM and annotated them using CYTO.

Combination therapy of PARPi and anti PD1 antibody showed increased effector T cell proportion in the sample S321

The immunocompetent samples were treated with 10 µg/ mL of pembrolizumab (anti PD1 antibody) or 20 µM Olaparib (PARPi) and their combination. There were 6 replicates for each of the conditions, including control. The specific values used for the experiment were decided as per previous experiments from the lab (Figure X - introduction). The drug treatments were done on day 1. The cells were harvested on day 3 of the drug treatment (post 72 hours), after which flow cytometry analysis was done. The cell proportions were obtained from clustering EpCam negative cells (non-tumour cells) using FlowSOM as described before.

In sample S321, increased effector T cell (Cytotoxic T cells and Helper T cells) proportions were seen in the combination of Olaparib and pembrolizumab compared to the control and monotherapy of these drugs (Figure 10). Monotherapy with Olaparib did not show a difference in the immune cell proportion compared to the control (Figure 10). Monotherapy with Pembrolizumab showed a slight increase in the effector T cell

proportion but not as much as in the combination (Figure 10). Sample S333 showed almost no difference between the immune cell proportion between the different treatment methods and control (Figure 10). A slight increase in the CD8+ T cells and CD56+ cells was seen in the monotherapy with Pembrolizumab 10 µg/ mL. in S263 (Figure 10).

CD8+ T cell functional activity was increased upon anti-PD1-antibody monotherapy and anti-PD1 antibody – PARPi combination therapy in sample S321

EpCam negative cells from treatments with 20 µM of Olaparib (PARPi) and 10 µg/ mL of Pembrolizumab (anti-PD1-antibody) and their combinations were clustered using FlowSOM, which were annotated to different cell types using CYTO. From this, the mean intensity of each marker per cluster was derived. This value was used to calculate the log₂ fold change in the functional marker per cell type between each of the treatments (– monotherapies of Olaparib (PARPi) and Pembrolizumab (anti-PD1-antibody) and their combination therapy) against the control.

For sample S321, the treatment with anti-PD1-antibody and the combination of PARPi and anti-PD1-antibody increased the GrzB expression in CD8+ T cells (Figure 11). Monotherapy treatment with the PARPi decreased the GrzB expression. The expression levels of IFN γ and Ki67 in CD8+ T cells revealed negligible variations during the monotherapies of PARPi and anti-PD1-antibody and their combination therapy. HLA-DR, IFN γ and Ki-67 expression levels in Dendritic cells also showed no substantial changes between these 3 treatment conditions and compared to control (Figure 11). In sample S333, a decrease in the HLA-DR expression was observed in macrophages for PARPi monotherapy compared to the control. HLA-DR expression further plummeted in the combination therapy of PARPi and anti-PD1-antibody. The sample S333 showed negligible changes in the functional activity between monotherapies of PARPi and anti-PD1-antibody, their combination therapy compared to control, in the other Immune cells. This is expected as sample S333 was unresponsive towards monotherapy of PARPi and anti-PD1-antibody and their combination (Figure 11). In sample S263, GrzB expression levels were slightly elevated in anti-Pd-1 antibody treatment (Figure 11). A decrease in GrzB expression was observed in CD8+ T cells in both PARPi treatment and combination treatment.

HLA-DR expression in CD11c+ cells were also observed to be decreased, especially in the treatment with anti-PD-antibody and the combination treatment.

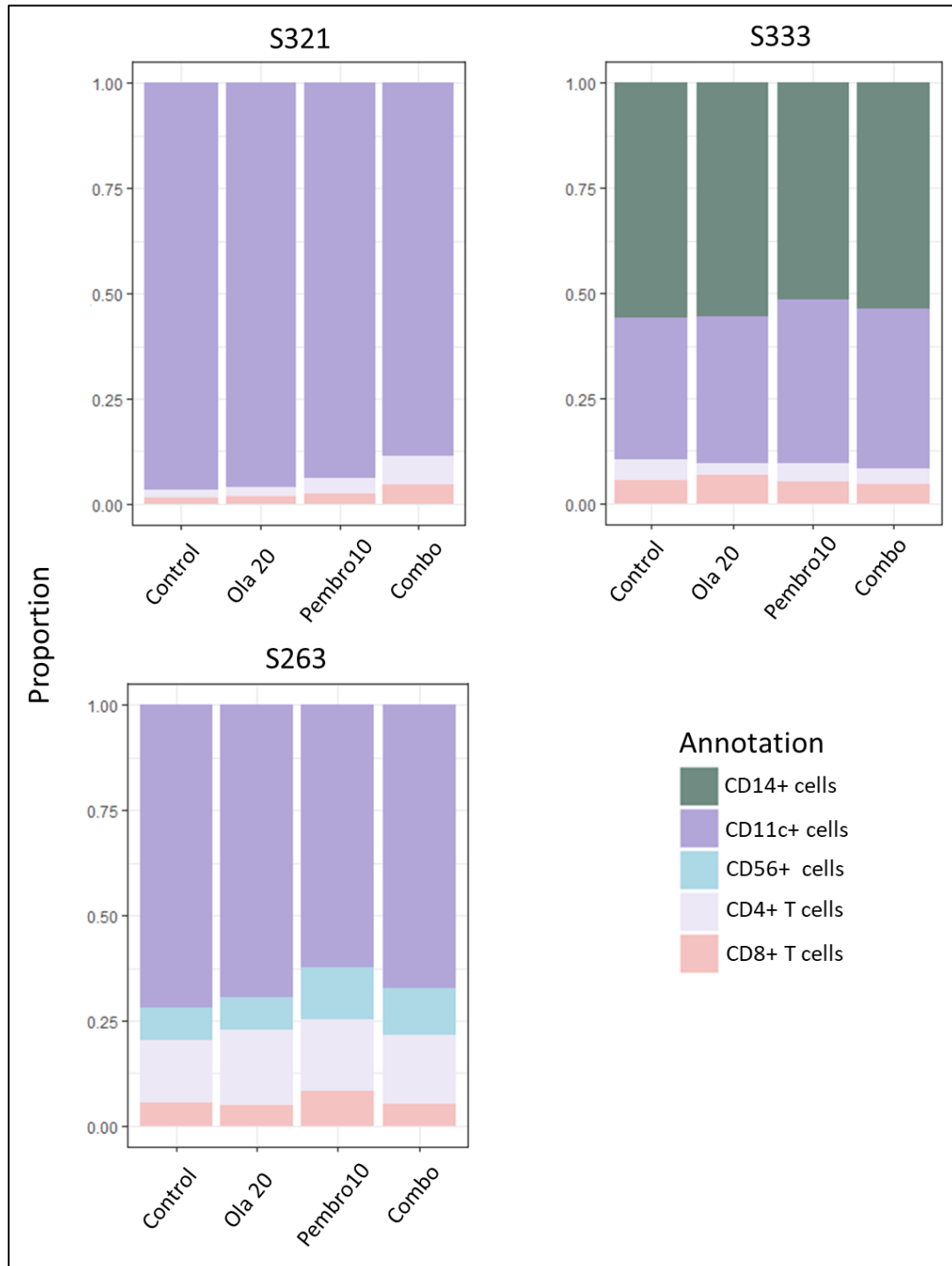


Figure 10: Immune cell proportion in the patient-derived immunocompetent cultures after treatment with 10 µg/ mL of pembrolizumab (anti PD1 antibody) or 20 µM Olaparib (PARPi) and their combination in samples S321, S333, S263. Each bar plot – S321, S333 and S263 shows the immune cell proportion obtained from flow cytometry on the day of tissue processing and the end of treatments (post 72

hours) with 10 µg/ mL of pembrolizumab (anti PD1 antibody) or 20 µM Olaparib (PARPi) and their combination. Proportions were obtained by clustering EpCam negative (non-tumour) cells using FlowSOM and annotated them using CYTO.

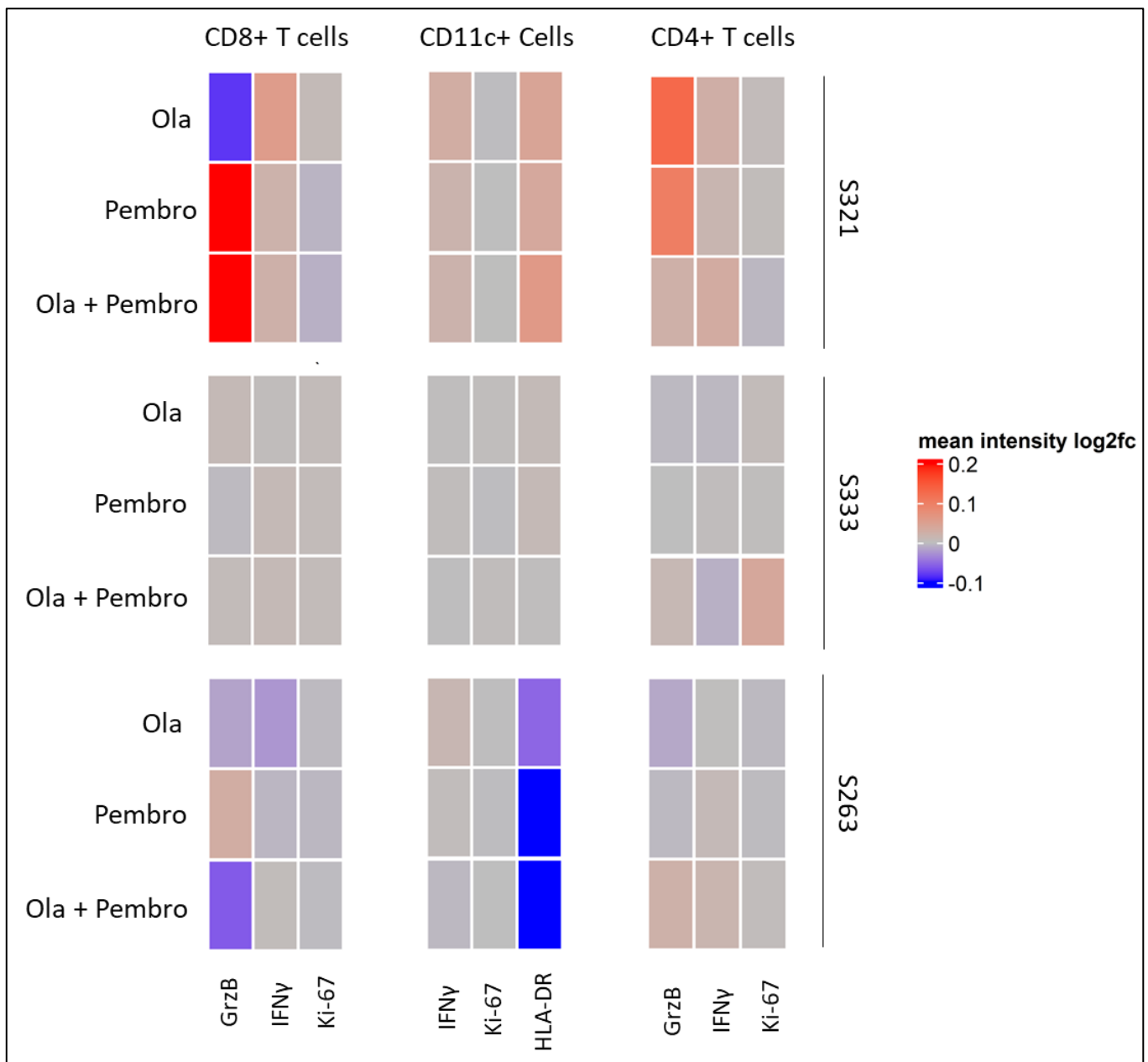


Figure 11: Immune cell Functional Activity of iPDCs of samples S321, S333 and S263 upon treatment with monotherapies of PARPi, Anti PD1 antibody and their combination. Treatment conditions performed were PARPi monotherapy – 20 µM of Olaparib (Ola), anti-PD1-antibody monotherapy – 10 µg/ mL of Pembrolizumab (Pembro) and their combination (Ola + Pembro). Functional activity of the immune cells were assessed by checking the levels of GrzB, IFN γ and Ki-67 for CD8+ T cells and IFN γ , Ki-67 and HLA-DR for CD11c+ cells. Each heatmap shows the log2 fold change of the immune cell functional markers for each cell type per treatment per sample.

Decreased effector T cell proportions were observed with increased concentration of ATRi in samples S321 and S263

The immunocompetent cultures were treated with 0.02 μM , 0.1 μM and 1 μM of Berzosertib/ VE-822 (ATRi) and they were harvested on day 3 for flow cytometry. A decreased effector T cell (Cytotoxic T cells and Helper T cells) proportion was observed with an increasing concentration of ATRi in sample S321 (Figure 12). An increased proportion of effector T cells compared to the control was observed in the lowest concentration (0.02 μM) of ATRi tested. Increasing the concentration to 0.1 μM decreased the effector T cell proportion (Figure 12). Sample S263 showed almost no difference in the immune cell proportion between the monotherapies of different concentrations of ATRi and control. The proportion of CD8+ T cells were also increased in ATRi concentrations of 0.02 μM . This proportion was further increased at a concentration of 0.1 μM (Figure 12). The proportions of CD8+ T cell was reduced significantly when the concentrations of ATRi was increased to 1 μM (Figure 12). There were negligible differences in the proportion of different immune cell types in ATRi treatment of different concentrations and control (Figure 12).

Decreased functional activity of CD8+ T cells exhibited a decline with increased concentration of ATRi

The immunocompetent cultures were treated with 0.02 μM , 0.1 μM and 1 μM of Berzosertib/ VE-822 (ATRi). The functional activity of all immune cells in sample S321 was observed to reduce when the concentrations of ATRi were increased (Figure 13). This is especially seen in the CD8+ T cells, where there is a substantial decrease in the expression levels of GrzB. Sample S333 showed no significant change in immune cell functional activity when the concentration of ATRi was increased (Figure 13). Similar to sample S321, sample S263 also showed a trend of decreasing GrzB expression with increasing concentrations of ATRi (Figure 13). Also, a decreased HLA-DR expression was observed in all concentrations of ATRi treatments in sample S263.

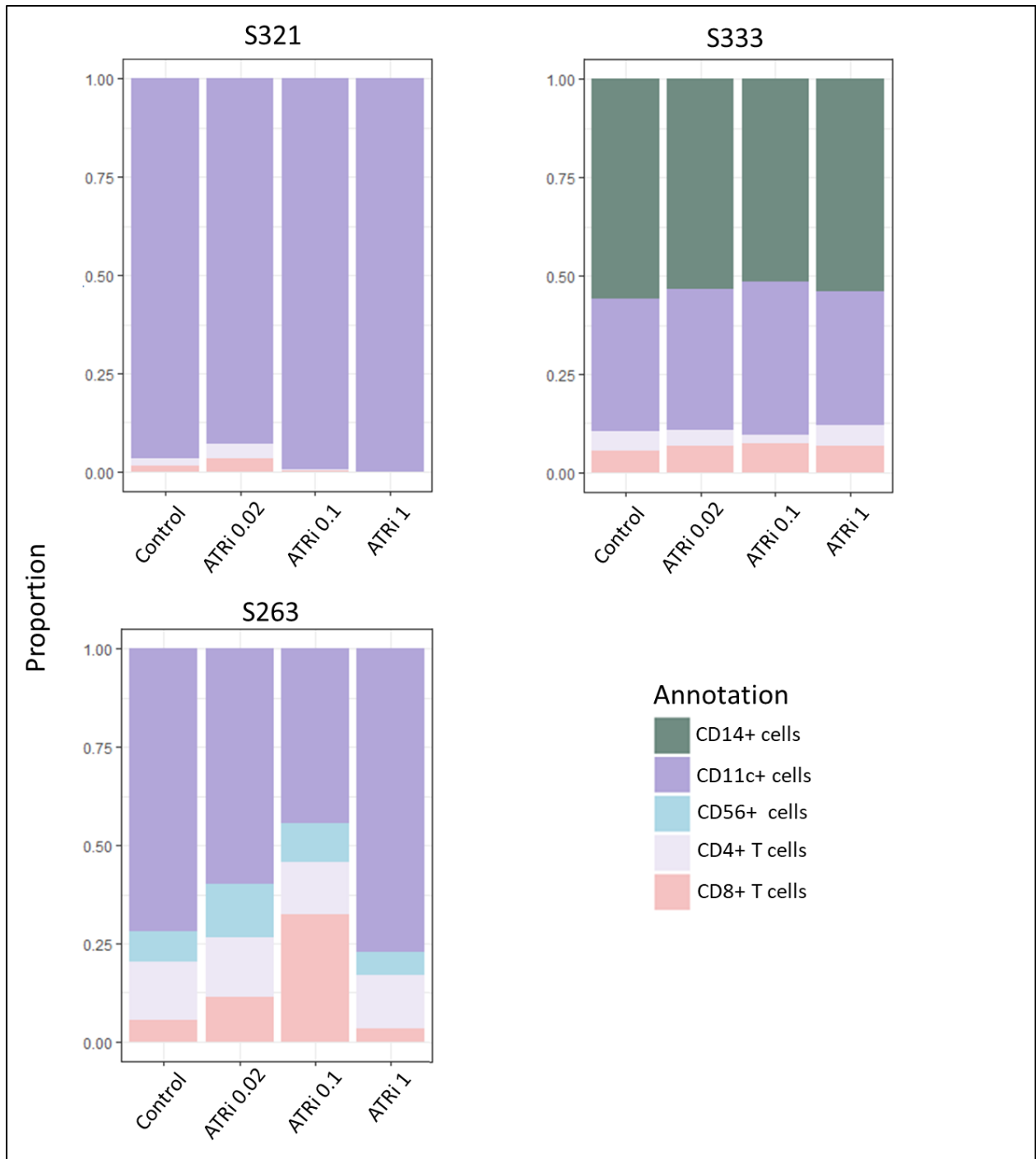


Figure 12: Immune cell proportion in the patient-derived immunocompetent cultures after treatment with 0.02 μ M, 0.1 μ M and 1 μ M of Berzosertib/ VE-822 (ATRi). Each bar plot – S321, S333 and S263 shows the immune cell proportion obtained from flow cytometry on the day of tissue processing and the end of treatments (post 72 hours) with 0.02 μ M, 0.1 μ M and 1 μ M of Berzosertib/ VE-822 (ATRi). Proportions were obtained by clustering EpCam negative (non-tumour) cells using FlowSOM and annotated them using CYTO.

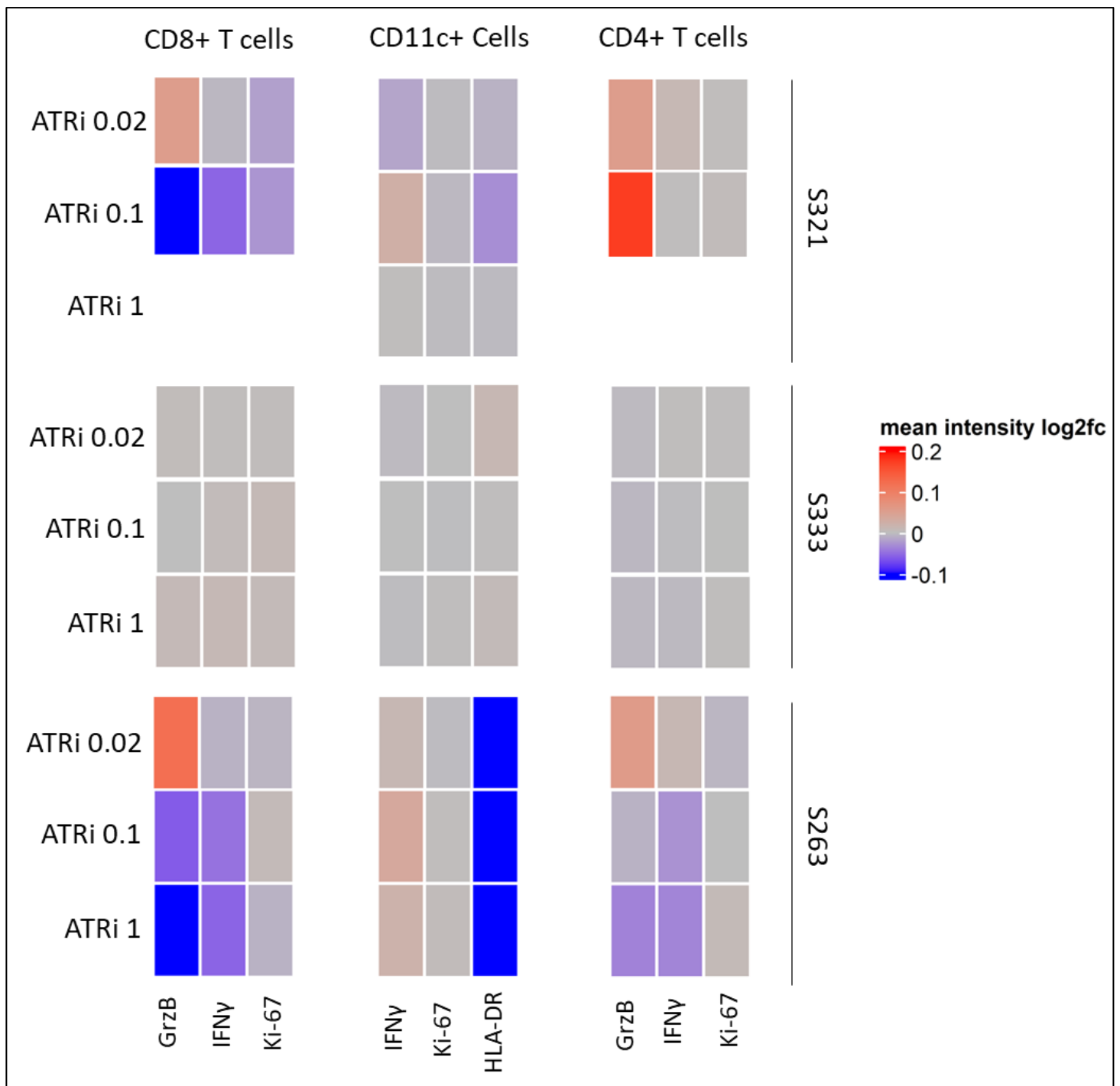


Figure 13: Immune cell Functional Activity of iPDCs of samples S321, S333 and S263 on administering them with monotherapies of ATRi. Treatment conditions performed were ATRi monotherapy – 0.02 μ M, 0.1 μ M and 1 μ M of Berzosertib/VE-822 (ATRi). Functional activity of the immune cells was assessed by checking the levels of GrzB, IFN γ and Ki-67 for CD8+ T cells and IFN γ , Ki-67 and HLA-DR for CD11c+ cells. Each heatmap shows the log2 fold change of the immune cell functional markers for each cell type per treatment per sample.

Highest effector T cell proportion in was seen in 0.2 μ M ATXi concentration

The immunocompetent cultures were treated with 0.13 μ M, 0.2 μ M and 0.7 μ M of Ziritaxestat/ GLPG1690 (ATXi). In the sample S321, monotherapy of ATXi 0.13 μ M showed almost negligible differences in effector T cell proportion compared to the control (Figure 14). On increasing this concentration to 0.2 μ M, we see a substantial increase in the proportion of effector T cells. Further increasing the concentration to 0.7 μ M led to a steep decrease in both the cell types of effector T cells. Sample S333 showed a slight decline in the effector T cell proportions for ATXi 0.7 μ M treatment. There were negligible differences between the immune cell proportions of the control and other ATXi treatments (Figure 14). Sample S263 showed similar effector T cell proportions to the control on treating with 0.2 μ M ATXi (Figure 14). The CD8+ T cell proportion in particular was substantially decreased when the concentration was increased to 0.7 μ M in sample S263.

Enhanced expression of GrzB was detected within CD8+ T cells in sample S321 following exposure to 0.2 μ M of ATXi

The immunocompetent cultures were treated with 0.13 μ M, 0.2 μ M and 0.7 μ M of Ziritaxestat/ GLPG1690 (ATXi). In sample S321, treatment with ATXi 0.13 μ M resulted in low immune cell activity. When the concentration of ATXi was increased to 0.2 μ M, there was an increase in the GrzB in CD8+ T cells, indicating enhanced functional activity (Figure 15). Increasing the concentration of ATXi further to 0.7 μ M instead caused a decrease in the GrzB expression. There was no substantial difference in the functional activity of CD11c+ cells between different monotherapies of ATXi with control. Sample S333 showed no significant change in immune cell functional activity when the concentration of ATXi was increased (Figure 15). In sample S263, GrzB expression in CD8+ T cells and HLA-DR expression in CD11c+ cells were markedly reduced in both 0.2 μ M and 0.7 μ M of ATXi monotherapy (Figure 15).

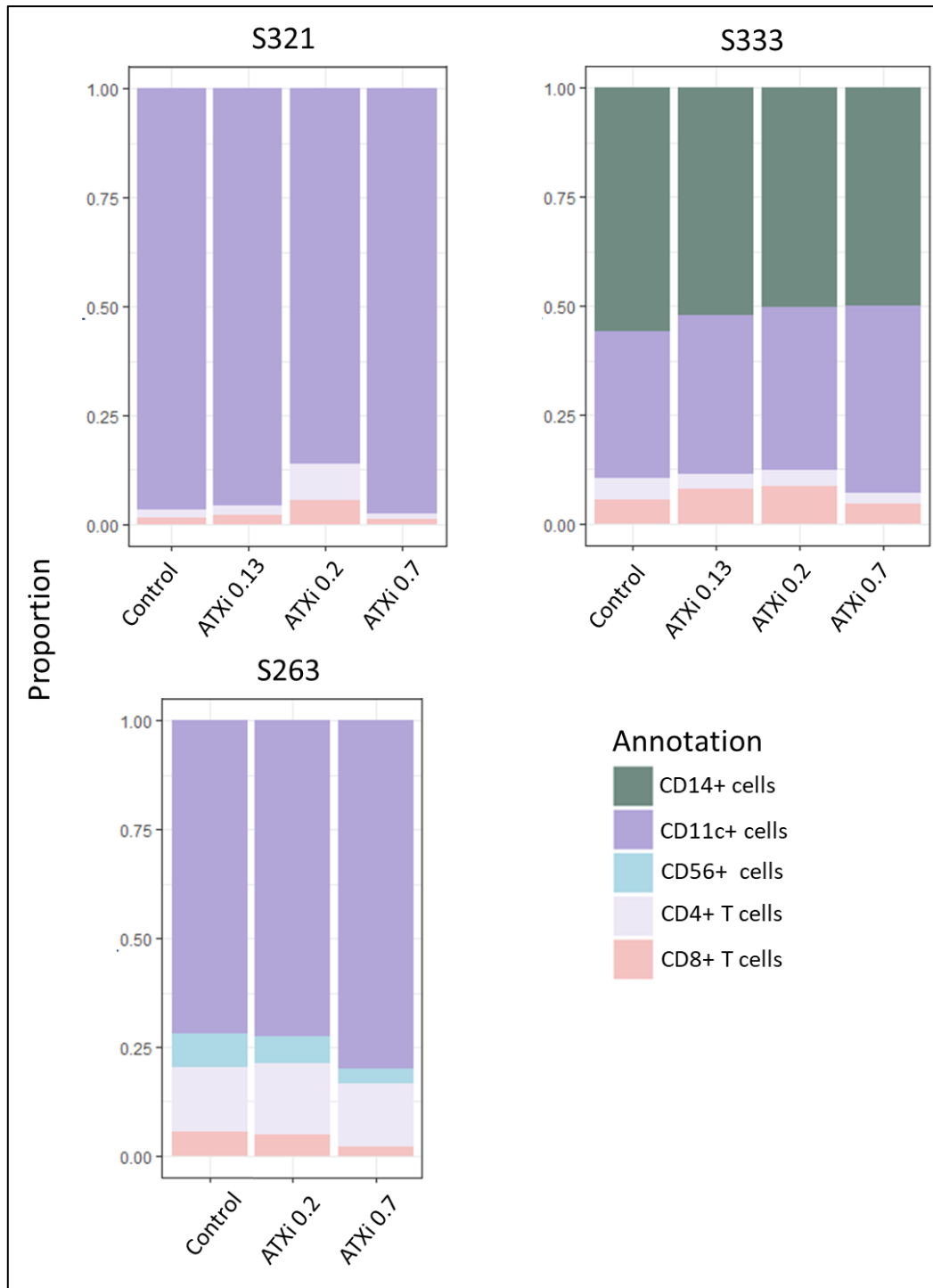


Figure 14: Immune cell proportion in the patient-derived immunocompetent cultures after treatment with 0.13 μM , 0.2 μM and 0.7 μM of Ziritaxestat/GLPG1690 (ATXi). Each bar plot – S321, S333 and S263, shows the immune cell proportion obtained from flow cytometry on the day of tissue processing and the end of treatments (post 72 hours) with 0.13 μM , 0.2 μM and 0.7 μM of Ziritaxestat/GLPG1690 (ATXi). Proportions were obtained by clustering EpCam negative (non-tumour) cells using FlowSOM and annotated them using CYTO.

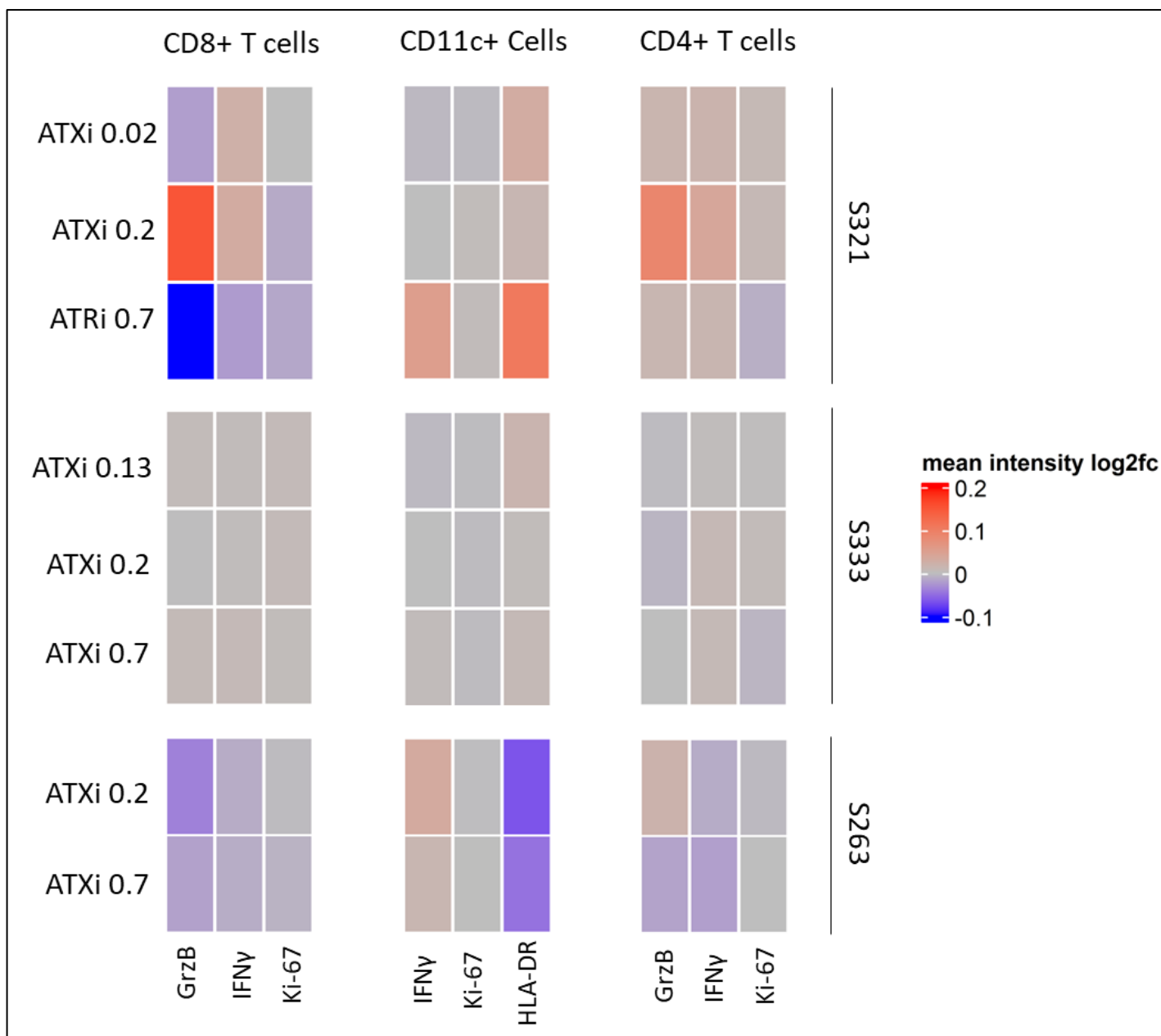


Figure 15: Immune cell Functional Activity of iPDCs of samples S321, S333 and S263 on administering them with monotherapies of ATXi. Treatment conditions performed were ATXi monotherapy – 0.13 μM , 0.2 μM and 0.7 μM of Ziritaxestat/GLPG1690 (ATXi). (just the latter two for S263). Functional activity of the immune cells was assessed by checking the levels of GrzB, IFN γ and Ki-67 for CD8+ T cells and IFN γ , Ki-67 and HLA-DR for CD11c+ cells. Each heatmap shows the log2 fold change of the immune cell functional markers for each cell type per treatment per sample.

Elevated proportions of CD8+ T cells were observed in samples S333 and S263 following administration of ATRi – ATXi combinations at higher concentrations

The immunocompetent cultures were treated with combinations of Berzosertib/ VE-822 (ATRi) and Ziritaxestat/ GLPG1690 (ATXi) - 0.02 μ M (ATRi) + 0.2 μ M (ATXi) (in S333 and S263), 0.02 μ M (ATRi) + 0.13 μ M (ATXi) (in S321), 0.1 μ M (ATRi) + 0.2 μ M (ATXi) (in S321, S333 and S263) and 1 μ M (ATRi) + 0.2 μ M (ATXi) (in S321 and S333). In sample S321, all the combinations - 0.02 μ M (ATRi) + 0.13 μ M (ATXi), 0.1 μ M (ATRi) + 0.2 μ M (ATXi) and 1 μ M (ATRi) + 0.2 μ M (ATXi), showed decreased effector T cell proportion, even in the treatment which had the combination of the lowest concentration of the 2 drugs (Figure 16). Sample S333 showed a slightly higher CD8+ T cell proportion on treatment with the highest concentration of the 2 drugs - 1 μ M (ATRi) + 0.2 μ M (ATXi) (Figure 16). Sample S263 showed a slightly higher proportion of CD8+ T cells in the combination of 0.1 μ M (ATRi) + 0.2 μ M (ATXi) (Figure 16). There were negligible differences between the immune cell proportions of the control and other combination treatments.

Functional activity of CD8+ T cells and CD11c+ cells was attenuated in combination therapies

The immunocompetent cultures were treated with combinations of Berzosertib/ VE-822 (ATRi) and Ziritaxestat/ GLPG1690 (ATXi) - 0.02 μ M (ATRi) + 0.2 μ M (ATXi) (in S333 and S263), 0.02 μ M (ATRi) + 0.13 μ M (ATXi) (in S321), 0.1 μ M (ATRi) + 0.2 μ M (ATXi) (in S321, S333 and S263) and 1 μ M (ATRi) + 0.2 μ M (ATXi) (in S321 and S333). In sample S321, the combination with the lowest concentration of both drugs - 0.02 μ M (ATRi) + 0.13 μ M (ATXi) showed a negligible increase in the functional activity of both CD8+ T cells and Dendritic cells. In the combination of 0.1 μ M (ATRi) + 0.2 μ M (ATXi), we see functional states resembling that of 0.1 μ M ATRi treatment (Figure 17). Sample S333 showed no significant change in immune cell functional activity between the combination treatments and control. Sample S263 showed increased GrzB expression in the combination - 0.02 μ M (ATRi) + 0.2 μ M (Figure 17). This decreased when the concentration of ATRi in the combination was increased - 0.1 μ M (ATRi) + 0.2 μ M. Decreased HLA-DR expression was also observed in both the combination treatments in sample S263 (Figure 17).

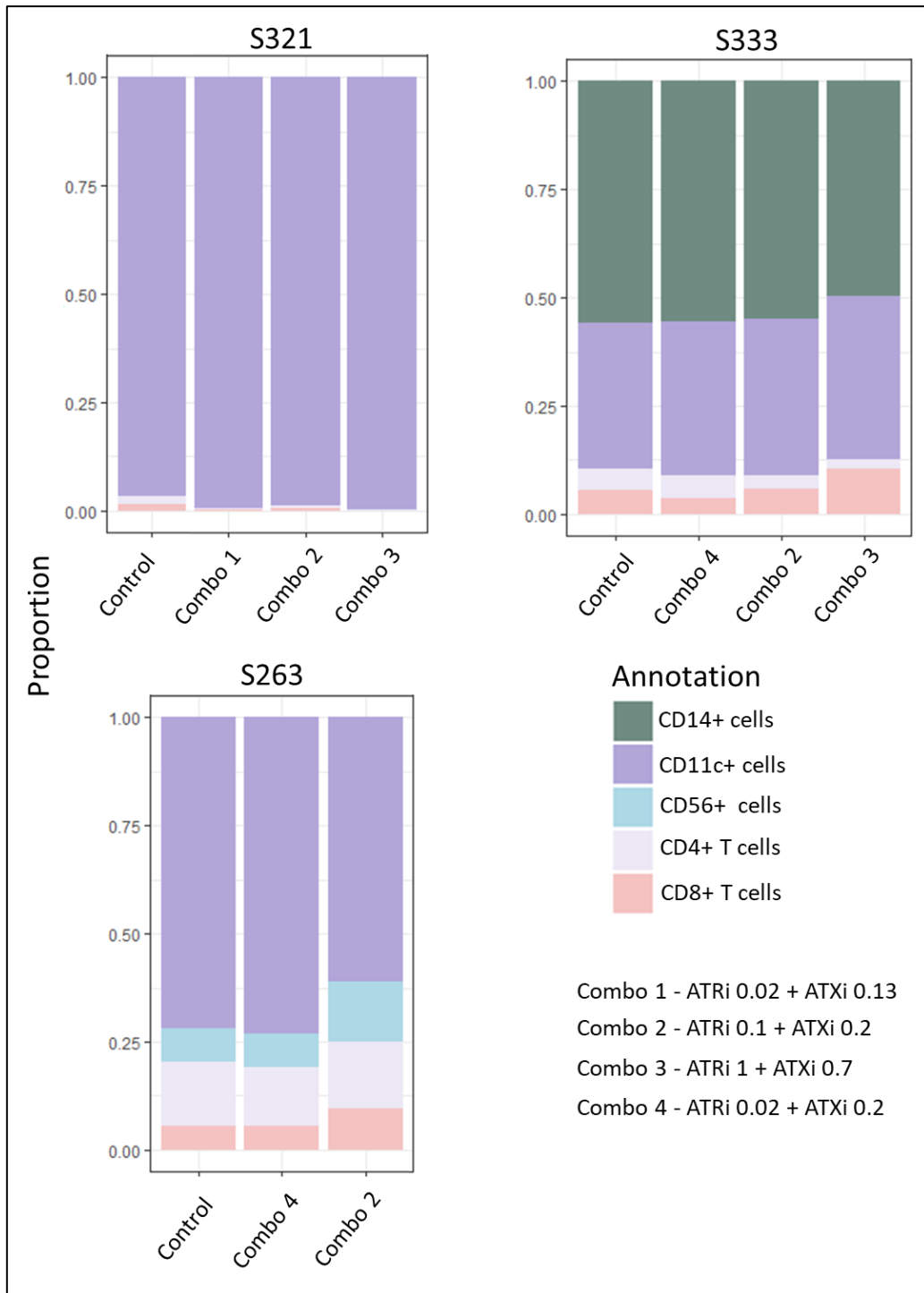


Figure 16: Immune cell proportion in the patient-derived immunocompetent cultures after treatment with combinations of Berzosertib/ VE-822 (ATRi) and Ziritaxestat/ GLPG1690 (ATXi). Each bar plot – S321, S333 and S263, shows the immune cell proportion obtained from flow cytometry on the day of tissue processing and the end of treatments (post 72 hours) with Combo 1 – ATRi 0.02 μ M + ATXi 0.13 μ M, Combo 2 – ATRi 0.1 μ M + ATXi 0.2 μ M, Combo 3 – ATRi 1 + ATXi 0.7, Combo 4 – ATRi 0.02 μ M + ATXi 0.2 μ M. Proportions were obtained by clustering EpCam negative (non-tumour) cells using FlowSOM and annotated them using CYTO.

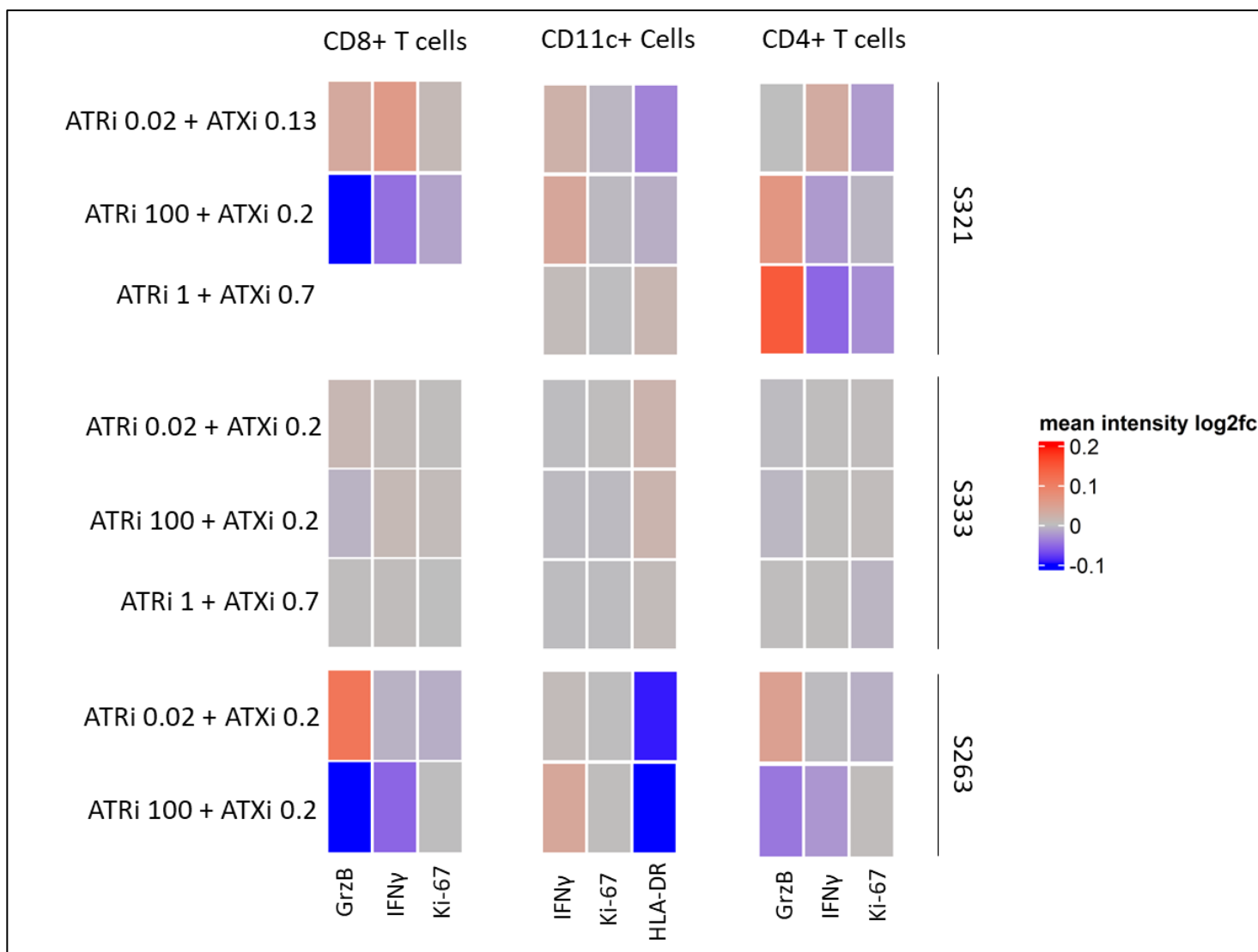


Figure 17: Immune cell Functional Activity of iPDCs of samples S321, S333 and S263 on administering them with ATRi-ATXi combination therapies. Treatment conditions (all concentrations are in μM) performed were **combinations of Berzosertib/ VE-822 (ATRi) and Ziritaxestat/ GLPG1690 (ATXi)**. Functional activity of the immune cells was assessed by checking the levels of GrzB, IFN γ and Ki-67 for CD8+ T cells and IFN γ , Ki-67 and HLA-DR for CD11c+ cells. Each heatmap shows the log₂ fold change of the immune cell functional markers for each cell type per treatment per sample.

Pronounced anti-tumour efficacy while maintaining minimal immune cell toxicity in the combinatorial treatment of 100 μM (ATRi) + 0.2 μM (ATXi)

iPDCs developed from sample S321, S333, S263 and were plated in 384 well plates were stained with Fixable Live-or-dye™ stain. The cells were then fixed with 4% paraformaldehyde. Each of the wells were stained with Hoechst, anti CK7 antibody, anti CD45 antibody, DCM. The Imaging was done in OperaPhenix Scanner. The images were exported, flattened and then ran on a customised cell profiler pipeline. Cell segments were split into tumour cells and immune cells based on their nuclei/ cell size using a threshold value of 2500. Intensity values from DCM were used to calculate tumour and immune cell death proportions. CK7+ DCM+ double positive fraction of CK7+ cells were taken as tumour cell death while CD45+ DCM+ double positive fraction of CD45+ cells were taken as immune cell death.

In sample S321, increased tumour killing was observed in the highest concentration of ATRi (1 μM) and in the combination of 0.1 μM (ATRi) + 0.2 μM (ATXi) (Figure 18). However, immune cell death observed in this combination was less than in 1 μM ATRi (Figure 19). Sample S333, had the highest tumour killing capacity upon treatment with ATRi 1 μM (Figure 18). We observe no significant change in the immune cell proportion in sample S333 (Figure 19). Sample S263 showed significant tumour cell death in the highest concentration of ATXi (0.7 μM) and in the combination of 0.1 μM (ATRi) + 0.2 μM (ATXi) (Figure 18). We observe no significant change in the immune cell proportion in sample S263 (Figure 19).

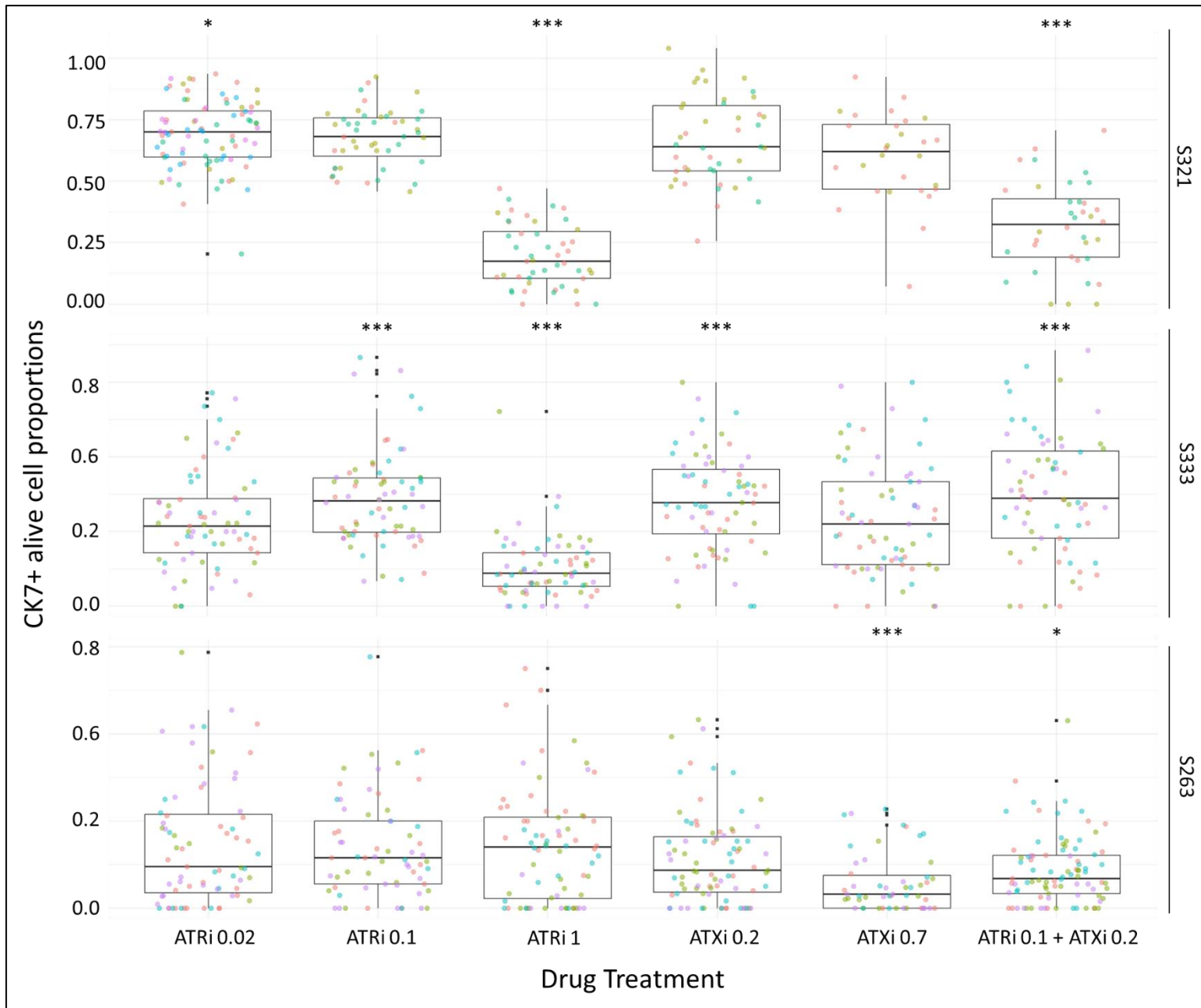


Figure 18: Boxplots showing proportion of CK7+ live cells normalised to control from iPDCs from S321, S333, S263. Treatment conditions (all concentrations are in μM) performed were **monotherapy of Berzosertib/ VE-822 (ATRi) and Ziritaxestat/ GLPG1690 (ATXi) and their combinations.** Tumour cell death was calculated using [CK7+ DCM+ cells/ all cells] from the intensities obtained from IF images. Each field in a well was taken as a single image and proportions for each of these images were calculated. * $P < 0.05$, *** $P < 0.001$.

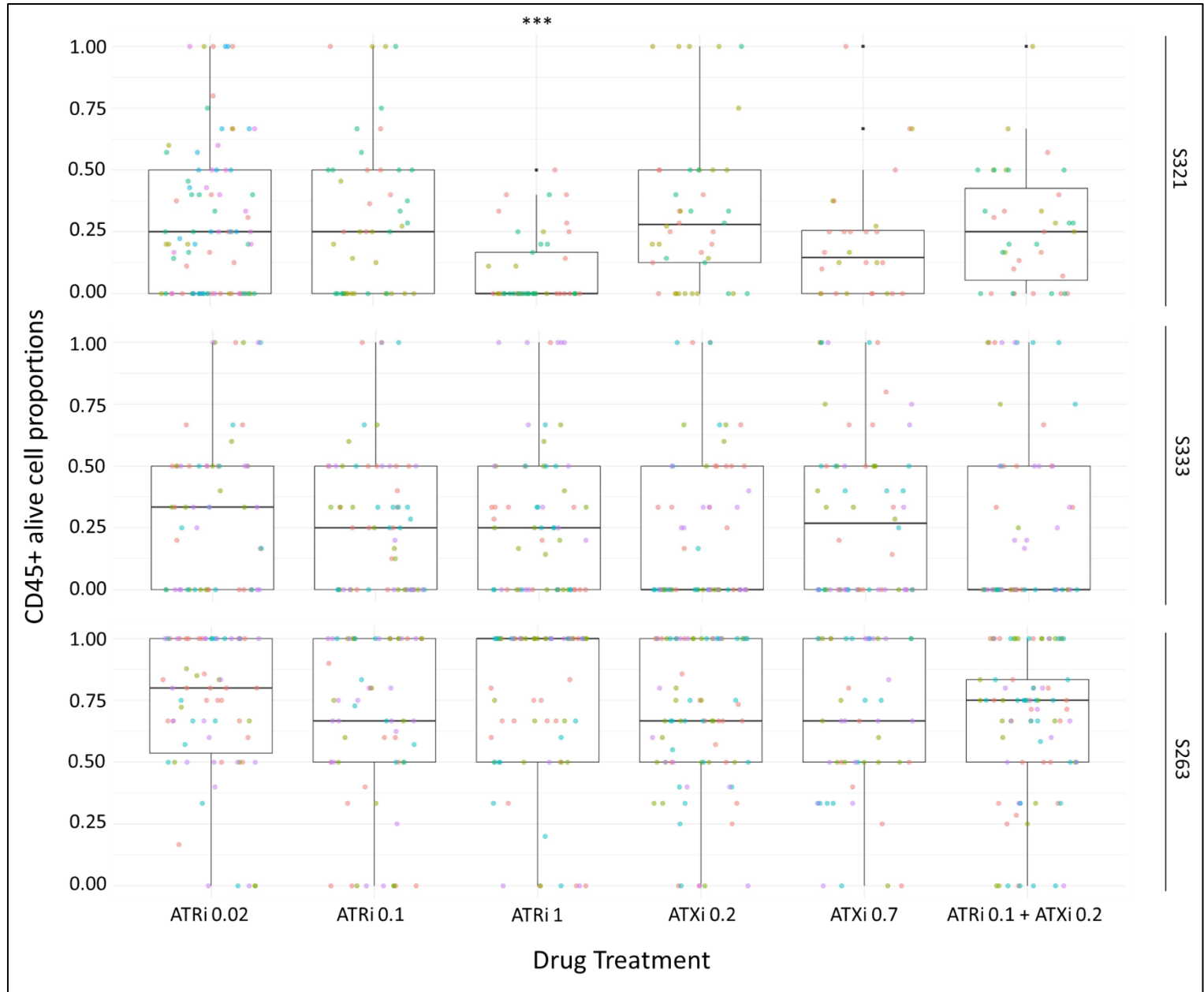


Figure 19: : Boxplots showing proportion of CD45+ live cells normalised to control from iPDCs from S321, S333, S263. Treatment conditions (all concentrations are in μM) performed were monotherapy of Berzosertib/ VE-822 (ATRi) and Ziritaxestat/ GLPG1690 (ATXi) and their combinations. Immune cell death was calculated using [CD45+ DCM+ cells/ all cells] from the intensities obtained from IF images. Each field in a well was taken as a single image and proportions for each of these images were calculated. *P<0.001.**

Discussion

Single-agent immunotherapies have shown very little promise in HGSOC patients. This prompts us to find an effective combination of drugs to be used and an ex vivo model which can recapitulate these results in the patients. Patient-derived immunocompetent cultures developed in the lab can give us more insights into the immune cells present in the tumour microenvironment, which can then be used to assess the efficacy of the drugs and drug combinations. We wanted to test the combination of Berzosertib/VE-822 (ATRi), which is a DNA-damaging drug and Ziritaxestat/GLPG1690 (ATXi), which is known to inhibit the LPA axis. Recent studies have also shown that LPA can act as an ovarian cancer activating factor and can have potent tumorigenic effects. It is also observed that LPA has a role in hypoxia-stimulated tumorigenic processes (Choi et al., 2010). These drugs are still in trials and have not yet been used in clinics. In theory, the ATRi acts by inhibiting the downstream function of ATR-mediated DNA damage response and repair pathway, while ATXi disrupts the enzymatic production of LPA, which is known to regulate immunological responses by modulating the functional activities of T cells and dendritic cells (Choi et al., 2010), (Bradbury et al., 2022). Already established DNA-damaging drug Olaparib (PARPi) and immunotherapy drug Pembrolizumab (anti-PD-1 antibody) were used to compare the treatment effect of ATRi and ATXi, whose effects on immune cell activities are not well characterized. Recent research findings have observed that LPA suppresses T-cell activity (Kremer et al., 2022). This may mean that ATXi can activate the CD8+ T cells. As mentioned before, the prognosis of an HGSOC patient depends greatly on whether it is immune barren, immune inactivated/unpenetrated or immune abundant, with the patients having immune abundant tumours showing the most response towards treatment. If an optimal combination that can mimic a similar immune constitution in the former two clinical subtypes can be titrated, it can substantially increase their prognosis.

Previous results from the lab showed that the dispase digestion was the most ideal for the dissociation of the tumour tissue. The dissociation using dispase was milder when compared to other tissue dissociation agents such as Collagenase and Hyaluronidase but is better for immune cell extractions and viability. One thing to note here is that the dispase digestion has limited efficacy in extracting larger immune cells such as fibroblasts and cancer associated fibroblasts (CAFs). This means that several components essential for pro tumour and anti tumour activity are not present in these cultures.

Omental samples showed better growth in the patient derived immunocompetent culture setup (iPDCs). Cell clumps in the cultures showed a higher increase in size in treatment free control compared to samples from other sources. Omental metastases are found to be common and more aggressive. This extensive growth may also be due to the constituents of the omental culture setup being made from tumour free omentum and the cells cultured in an environment closer to their origin.

All the immune cells in the day 0 is recapitulated in the cultures, albeit in a different proportion. We see an increase in the myeloid cell proportion in the cultures when

compared to day 0. This is extremely pronounced in sample S263, where the proportion of CD11c+ cells are of a minority, but it increased substantially in the day 3 control and even in different treatments. This might mean that the culture setup is more accommodating towards myeloid cell population. Presence of CD4+ T cells have been seen to increase the robustness and survival of CD8+ T cells in the cultures, which is expected from previous studies(Tay et al., 2021). Already clinically approved drugs such as Olaparib (PARPi), Pembrolizumab (anti PD1 antibody) and their combination was used in our panel to validate the extent of results in the other drugs which are novel. The fold change values in the functional activity of the samples between novel treatments and the control might appear to be very small, but if this is comparable in magnitude to the already established drugs, the small magnitude might be because of the dampening affect brought about by the system rather than the ineffectiveness of the drug. The ranges of this fold change also vary highly between different samples.

Immunofluorescence was used to calculate Tumour death in the cultures. This is because they cannot be assessed using flow data as most tumour cells are present as spheroids/ organoids in the cultures. During flow analysis, we usually only consider single cells due to the presence of debris and to prevent the overlap of multiple types of cells and thus expression signals. Thus, both tumour cell death and immune cell death proportion was calculated using DCM intensity. Increased concentration of ATRi increased both tumour and immune cell death in the cultures. Interestingly, increased concentration of ATXi also increased the death and exhaustion of immune cells, which is antagonistic to its function. This might be because the increased concentration of the drug is affecting other metabolic processes of the immune cell.

HGSOC is a subtype which has a high inter tumour heterogeneity. It has been observed that the different regions of the same sample have genetically and epigenetically different, with a highly varying transcriptome (literature and from the lab). This also means that the results we obtain from patient derived cultures will be having patient specific variations in them. This can be very easily understood by checking the difference in immune cell proportions between all the samples. All the immune cell types were recapitulated in iPDC control w.r.t the day 0 sample, but we do not see the same immune cell types across all the patient samples. This becomes even more pronounced when different treatments are administered to the culture. The functional activity of the immune cells and the tumour killing efficacy of each of the treatment methods also showed a large degree of variation across samples. The project in the beginning had an idea of using cultures from 50 different patients to provide more generalized observation and better statistics. Due to the lack of samples in flow and due to the poor quality of the tumour tissue, the number of samples used in this project was limited to 3. In future, we hope to include more samples to observe and provide more generalized and less patient specific results.

This project helps concrete the use of patient derived immunocompetent cultures as a model system to study the efficacy of various DNA damaging and immunotherapy drugs and their combination. As the cells for the culture are freshly derived from the patient tumour tissue and cultured in a physiologically relevant omentum gel matrix, it can better recapitulate the environment the tumour cells and immune cells of the native tumour. Recently announced FDA 2.0 states the removal of the requirement of animal

models as part of drug screening and development. Also, in the case of immunotherapy, it is difficult to have commendable translation between murine models and clinics due to the difference in immune cell/ modulator composition (Mestas & Hughes, 2004). This further increases the possibility of using patient derived immunocompetent cultures for assessing drugs and drug combinations, especially in cancers such as HGSOC which show minimal response to immunotherapies.

References

- SEER Ovarian Cancer. (2018, May 26). Available Online:
<https://Seer.Cancer.Gov/Statfacts/Html/Ovary.Html>.
- Aoki, J. (2004). Mechanisms of lysophosphatidic acid production. *Seminars in Cell & Developmental Biology*, 15(5), 477–489. <https://doi.org/10.1016/j.semcdb.2004.05.001>
- Ashwini S Nagaraj, Matilda Salko, Aditi Sirsikar, Erdogan Pekcan Erkan, Elina A Pietilä, Iga Niemiec, Jie Bao, Giovanni Marchi, Angéla Szabó, Kirsten Nowlan, Sanna Pikkusaari, Anna Kanerva, Johanna Tapper, Riitta Koivisto-Korander, Liisa Kauppi, Sampsa Hautaniemi, Anna Vähärautio, Jing Tang, Ulla-Maija Haltia, ... Anniina Färkkilä. (2024). Patient-derived functional immunology platform identifies responders to ATR inhibitor and immunotherapy combinations in ovarian cancer. *BioRxiv*.
- Audeh, M. W., Carmichael, J., Penson, R. T., Friedlander, M., Powell, B., Bell-McGuinn, K. M., Scott, C., Weitzel, J. N., Oaknin, A., Loman, N., Lu, K., Schmutzler, R. K., Matulonis, U., Wickens, M., & Tutt, A. (2010). Oral poly(ADP-ribose) polymerase inhibitor olaparib in patients with BRCA1 or BRCA2 mutations and recurrent ovarian cancer: a proof-of-concept trial. *The Lancet*, 376(9737), 245–251. [https://doi.org/10.1016/S0140-6736\(10\)60893-8](https://doi.org/10.1016/S0140-6736(10)60893-8)
- Baci, D., Bosi, A., Gallazzi, M., Rizzi, M., Noonan, D. M., Poggi, A., Bruno, A., & Mortara, L. (2020). The Ovarian Cancer Tumor Immune Microenvironment (TIME) as Target for Therapy: A Focus on Innate Immunity Cells as Therapeutic Effectors. *International Journal of Molecular Sciences*, 21(9), 3125. <https://doi.org/10.3390/ijms21093125>
- Bradbury, A., Zenke, F. T., Curtin, N. J., & Drew, Y. (2022). The Role of ATR Inhibitors in Ovarian Cancer: Investigating Predictive Biomarkers of Response. *Cells*, 11(15), 2361. <https://doi.org/10.3390/cells11152361>
- Brown, J. S., Sundar, R., & Lopez, J. (2018). Combining DNA damaging therapeutics with immunotherapy: more haste, less speed. *British Journal of Cancer*, 118(3), 312–324. <https://doi.org/10.1038/bjc.2017.376>
- Casado, J., Lehtonen, O., Rantanen, V., Kaipio, K., Pasquini, L., Häkkinen, A., Petrucci, E., Hynninen, J., Hietanen, S., Carpén, O., Biffoni, M., Färkkilä, A., & Hautaniemi, S. (2021). Agile workflow for interactive analysis of mass cytometry data. *Bioinformatics (Oxford, England)*, 37(9), 1263–1268. <https://doi.org/10.1093/bioinformatics/btaa946>
- Chen, D. S., & Mellman, I. (2017). Elements of cancer immunity and the cancer–immune set point. *Nature*, 541(7637), 321–330. <https://doi.org/10.1038/nature21349>
- Choi, J. W., Herr, D. R., Noguchi, K., Yung, Y. C., Lee, C.-W., Mutoh, T., Lin, M.-E., Teo, S. T., Park, K. E., Mosley, A. N., & Chun, J. (2010). LPA Receptors: Subtypes and Biological Actions. *Annual Review of Pharmacology and Toxicology*, 50(1), 157–186. <https://doi.org/10.1146/annurev.pharmtox.010909.105753>
- Cojocaru, E., Parkinson, C. A., & Brenton, J. D. (2018). Personalising Treatment for High-Grade Serous Ovarian Carcinoma. *Clinical Oncology*, 30(8). <https://doi.org/10.1016/j.clon.2018.05.008>
- Colombo, P. E., Fabbro, M., Theillet, C., Bibeau, F., Rouanet, P., & Ray-Coquard, I. (2014). Sensitivity and resistance to treatment in the primary management of epithelial ovarian cancer. In *Critical*

Reviews in Oncology/Hematology (Vol. 89, Issue 2).
<https://doi.org/10.1016/j.critrevonc.2013.08.017>

- Colombo, P.-E., Fabbro, M., Theillet, C., Bibeau, F., Rouanet, P., & Ray-Coquard, I. (2014). Sensitivity and resistance to treatment in the primary management of epithelial ovarian cancer. *Critical Reviews in Oncology/Hematology*, 89(2), 207–216.
<https://doi.org/10.1016/j.critrevonc.2013.08.017>
- de Bono, J., Mateo, J., Fizazi, K., Saad, F., Shore, N., Sandhu, S., Chi, K. N., Sartor, O., Agarwal, N., Olmos, D., Thiery-Vuillemin, A., Twardowski, P., Mehra, N., Goessl, C., Kang, J., Burgents, J., Wu, W., Kohlmann, A., Adelman, C. A., & Hussain, M. (2020). Olaparib for Metastatic Castration-Resistant Prostate Cancer. *New England Journal of Medicine*, 382(22), 2091–2102.
<https://doi.org/10.1056/NEJMoa1911440>
- Dudek, A. M., Martin, S., Garg, A. D., & Agostinis, P. (2013). Immature, Semi-Mature, and Fully Mature Dendritic Cells: Toward a DC-Cancer Cells Interface That Augments Anticancer Immunity. *Frontiers in Immunology*, 4. <https://doi.org/10.3389/fimmu.2013.00438>
- Duraiswamy, J., Turrini, R., Minasyan, A., Barras, D., Crespo, I., Grimm, A. J., Casado, J., Genolet, R., Benedetti, F., Wicky, A., Ioannidou, K., Castro, W., Neal, C., Moriot, A., Renaud-Tissot, S., Anstett, V., Fahr, N., Tanyi, J. L., Eiva, M. A., ... Coukos, G. (2021). Myeloid antigen-presenting cell niches sustain antitumor T cells and license PD-1 blockade via CD28 costimulation. *Cancer Cell*, 39(12), 1623-1642.e20. <https://doi.org/10.1016/j.ccell.2021.10.008>
- Emo, J., Meednu, N., Chapman, T. J., Rezaee, F., Balys, M., Randall, T., Rangasamy, T., & Georas, S. N. (2012). Lpa2 is a negative regulator of both dendritic cell activation and murine models of allergic lung inflammation. *Journal of Immunology (Baltimore, Md. : 1950)*, 188(8), 3784–3790.
<https://doi.org/10.4049/jimmunol.1102956>
- Färkkilä, A., Gulhan, D. C., Casado, J., Jacobson, C. A., Nguyen, H., Kochupurakkal, B., Maliga, Z., Yapp, C., Chen, Y.-A., Schapiro, D., Zhou, Y., Graham, J. R., Dezube, B. J., Munster, P., Santagata, S., Garcia, E., Rodig, S., Lako, A., Chowdhury, D., ... Konstantinopoulos, P. A. (2020). Immunogenomic profiling determines responses to combined PARP and PD-1 inhibition in ovarian cancer. *Nature Communications*, 11(1), 1459. <https://doi.org/10.1038/s41467-020-15315-8>
- Francisco, L. M., Sage, P. T., & Sharpe, A. H. (2010). The PD-1 pathway in tolerance and autoimmunity. *Immunological Reviews*, 236(1), 219–242. <https://doi.org/10.1111/j.1600-065X.2010.00923.x>
- Goode, E. L., Block, M. S., Kalli, K. R., Vierkant, R. A., Chen, W., Fogarty, Z. C., Gentry-Maharaj, A., Toloczko, A., Hein, A., Bouligny, A. L., Jensen, A., Osorio, A., Hartkopf, A. D., Ryan, A., Chudecka-Glaz, A., Magliocco, A. M., Hartmann, A., Jung, A. Y., Gao, B., ... Ramus, S. J. (2017). Dose-Response Association of CD8⁺ Tumor-Infiltrating Lymphocytes and Survival Time in High-Grade Serous Ovarian Cancer. *JAMA Oncology*, 3(12), e173290.
<https://doi.org/10.1001/jamaoncol.2017.3290>
- Herrera, F. G., Ronet, C., Ochoa de Olza, M., Barras, D., Crespo, I., Andreatta, M., Corria-Osorio, J., Spill, A., Benedetti, F., Genolet, R., Orcurto, A., Imbimbo, M., Ghisoni, E., Navarro Rodrigo, B., Berthold, D. R., Sarivalasis, A., Zaman, K., Duran, R., Dromain, C., ... Coukos, G. (2022). Low-Dose Radiotherapy Reverses Tumor Immune Desertification and Resistance to Immunotherapy. *Cancer Discovery*, 12(1), 108–133. <https://doi.org/10.1158/2159-8290.CD-21-0003>

- Hill, S. J., Decker, B., Roberts, E. A., Horowitz, N. S., Muto, M. G., Worley, M. J., Feltmate, C. M., Nucci, M. R., Swisher, E. M., Nguyen, H., Yang, C., Morizane, R., Kochupurakkal, B. S., Do, K. T., Konstantinopoulos, P. A., Liu, J. F., Bonventre, J. V., Matulonis, U. A., Shapiro, G. I., ... D'Andrea, A. D. (2018). Prediction of DNA Repair Inhibitor Response in Short-Term Patient-Derived Ovarian Cancer Organoids. *Cancer Discovery*, *8*(11), 1404–1421. <https://doi.org/10.1158/2159-8290.CD-18-0474>
- Integrated genomic analyses of ovarian carcinoma. (2011). *Nature*, *474*(7353), 609–615. <https://doi.org/10.1038/nature10166>
- Jemal, A., Bray, F., & Ferlay, J. (1999). Global Cancer Statistics: 2011. *CA Cancer J Clin*, *49*(2). <https://doi.org/10.3322/caac.20107>. Available
- Kandalaft, L. E., Dangaj Laniti, D., & Coukos, G. (2022). Immunobiology of high-grade serous ovarian cancer: lessons for clinical translation. *Nature Reviews Cancer*, *22*(11), 640–656. <https://doi.org/10.1038/s41568-022-00503-z>
- Konstantinopoulos, P. A., Waggoner, S., Vidal, G. A., Mita, M., Moroney, J. W., Holloway, R., Van Le, L., Sachdev, J. C., Chapman-Davis, E., Colon-Otero, G., Penson, R. T., Matulonis, U. A., Kim, Y. B., Moore, K. N., Swisher, E. M., Färkkilä, A., D'Andrea, A., Stringer-Reasor, E., Wang, J., ... Munster, P. (2019). Single-Arm Phases 1 and 2 Trial of Niraparib in Combination With Pembrolizumab in Patients With Recurrent Platinum-Resistant Ovarian Carcinoma. *JAMA Oncology*, *5*(8), 1141. <https://doi.org/10.1001/jamaoncol.2019.1048>
- Kremer, K. N., Buser, A., Thumkeo, D., Narumiya, S., Jacobelli, J., Pelanda, R., & Torres, R. M. (2022). LPA suppresses T cell function by altering the cytoskeleton and disrupting immune synapse formation. *Proceedings of the National Academy of Sciences*, *119*(15). <https://doi.org/10.1073/pnas.2118816119>
- Kulbe, H., Chakravarty, P., Leinster, D. A., Charles, K. A., Kwong, J., Thompson, R. G., Coward, J. I., Schioppa, T., Robinson, S. C., Gallagher, W. M., Galletta, L., Salako, M. A., Smyth, J. F., Hagemann, T., Brennan, D. J., Bowtell, D. D., & Balkwill, F. R. (2012). A Dynamic Inflammatory Cytokine Network in the Human Ovarian Cancer Microenvironment. *Cancer Research*, *72*(1), 66–75. <https://doi.org/10.1158/0008-5472.CAN-11-2178>
- Kwok, M., Davies, N., Agathangelou, A., Smith, E., Oldreive, C., Petermann, E., Stewart, G., Brown, J., Lau, A., Pratt, G., Parry, H., Taylor, M., Moss, P., Hillmen, P., & Stankovic, T. (2016). ATR inhibition induces synthetic lethality and overcomes chemoresistance in TP53- or ATM-defective chronic lymphocytic leukemia cells. *Blood*, *127*(5), 582–595. <https://doi.org/10.1182/blood-2015-05-644872>
- Lei, X., Lei, Y., Li, J.-K., Du, W.-X., Li, R.-G., Yang, J., Li, J., Li, F., & Tan, H.-B. (2020). Immune cells within the tumor microenvironment: Biological functions and roles in cancer immunotherapy. *Cancer Letters*, *470*, 126–133. <https://doi.org/10.1016/j.canlet.2019.11.009>
- Lengyel, E. (2010). Ovarian Cancer Development and Metastasis. *The American Journal of Pathology*, *177*(3), 1053–1064. <https://doi.org/10.2353/ajpath.2010.100105>
- Li, X., Shao, C., Shi, Y., & Han, W. (2018). Lessons learned from the blockade of immune checkpoints in cancer immunotherapy. *Journal of Hematology & Oncology*, *11*(1), 31. <https://doi.org/10.1186/s13045-018-0578-4>

- Lisio, M.-A., Fu, L., Goyeneche, A., Gao, Z., & Telleria, C. (2019). High-Grade Serous Ovarian Cancer: Basic Sciences, Clinical and Therapeutic Standpoints. *International Journal of Molecular Sciences*, *20*(4), 952. <https://doi.org/10.3390/ijms20040952>
- Massagué, J. (2004). G1 cell-cycle control and cancer. *Nature*, *432*(7015), 298–306. <https://doi.org/10.1038/nature03094>
- Mempel, T. R., Henrickson, S. E., & von Andrian, U. H. (2004). T-cell priming by dendritic cells in lymph nodes occurs in three distinct phases. *Nature*, *427*(6970), 154–159. <https://doi.org/10.1038/nature02238>
- Mestas, J., & Hughes, C. C. W. (2004). Of Mice and Not Men: Differences between Mouse and Human Immunology. *The Journal of Immunology*, *172*(5), 2731–2738. <https://doi.org/10.4049/jimmunol.172.5.2731>
- Meza-Perez, S., & Randall, T. D. (2017). Immunological Functions of the Omentum. *Trends in Immunology*, *38*(7), 526–536. <https://doi.org/10.1016/j.it.2017.03.002>
- Momenimovahed, Z., Tiznobaik, A., Taheri, S., & Salehiniya, H. (2019). Ovarian cancer in the world: Epidemiology and risk factors. In *International Journal of Women's Health* (Vol. 11). <https://doi.org/10.2147/IJWH.S197604>
- Morand, S., Devanaboyina, M., Staats, H., Stanbery, L., & Nemunaitis, J. (2021). Ovarian cancer immunotherapy and personalized medicine. In *International Journal of Molecular Sciences* (Vol. 22, Issue 12). <https://doi.org/10.3390/ijms22126532>
- Nero, C., Vizzielli, G., Lorusso, D., Cesari, E., Daniele, G., Loverro, M., Scambia, G., & Sette, C. (2021a). Patient-derived organoids and high grade serous ovarian cancer: from disease modeling to personalized medicine. In *Journal of Experimental and Clinical Cancer Research* (Vol. 40, Issue 1). <https://doi.org/10.1186/s13046-021-01917-7>
- Nero, C., Vizzielli, G., Lorusso, D., Cesari, E., Daniele, G., Loverro, M., Scambia, G., & Sette, C. (2021b). Patient-derived organoids and high grade serous ovarian cancer: from disease modeling to personalized medicine. *Journal of Experimental & Clinical Cancer Research*, *40*(1), 116. <https://doi.org/10.1186/s13046-021-01917-7>
- Perets, R., Wyant, G. A., Muto, K. W., Bijron, J. G., Poole, B. B., Chin, K. T., Chen, J. Y. H., Ohman, A. W., Stepule, C. D., Kwak, S., Karst, A. M., Hirsch, M. S., Setlur, S. R., Crum, C. P., Dinulescu, D. M., & Drapkin, R. (2013). Transformation of the Fallopian Tube Secretory Epithelium Leads to High-Grade Serous Ovarian Cancer in Brca;Tp53;Pten Models. *Cancer Cell*, *24*(6), 751–765. <https://doi.org/10.1016/j.ccr.2013.10.013>
- Perez-Villatoro, F., Oikkonen, J., Casado, J., Chernenko, A., Gulhan, D. C., Tumiati, M., Li, Y., Lavikka, K., Hietanen, S., Hynninen, J., Haltia, U.-M., Tyrmi, J. S., Laivuori, H., Konstantinopoulos, P. A., Hautaniemi, S., Kauppi, L., & Färkkilä, A. (2022). Optimized detection of homologous recombination deficiency improves the prediction of clinical outcomes in cancer. *Npj Precision Oncology*, *6*(1), 96. <https://doi.org/10.1038/s41698-022-00339-8>
- Polterauer, S., Vergote, I., Concin, N., Braicu, I., Chakerov, R., Mahner, S., Woelber, L., Cadron, I., Van Gorp, T., Zeillinger, R., Castillo-Tong, D. C., & Sehouli, J. (2012). Prognostic Value of Residual Tumor Size in Patients With Epithelial Ovarian Cancer FIGO Stages IIA–IV: Analysis of the OVCAD Data. *International Journal of Gynecologic Cancer*, *22*(3), 380–385. <https://doi.org/10.1097/IGC.0b013e31823de6ae>

- Rose, M., Burgess, J. T., O'Byrne, K., Richard, D. J., & Bolderson, E. (2020). PARP Inhibitors: Clinical Relevance, Mechanisms of Action and Tumor Resistance. *Frontiers in Cell and Developmental Biology*, 8. <https://doi.org/10.3389/fcell.2020.564601>
- Saldivar, J. C., Cortez, D., & Cimprich, K. A. (2017). The essential kinase ATR: ensuring faithful duplication of a challenging genome. *Nature Reviews Molecular Cell Biology*, 18(10), 622–636. <https://doi.org/10.1038/nrm.2017.67>
- Stewart, C., Ralyea, C., & Lockwood, S. (2019). Ovarian Cancer: An Integrated Review. *Seminars in Oncology Nursing*, 35(2), 151–156. <https://doi.org/10.1016/j.soncn.2019.02.001>
- Sun, C., Mezzadra, R., & Schumacher, T. N. (2018). Regulation and Function of the PD-L1 Checkpoint. *Immunity*, 48(3), 434–452. <https://doi.org/10.1016/j.immuni.2018.03.014>
- Sung, H., Ferlay, J., Siegel, R. L., Laversanne, M., Soerjomataram, I., Jemal, A., & Bray, F. (2021). Global Cancer Statistics 2020: GLOBOCAN Estimates of Incidence and Mortality Worldwide for 36 Cancers in 185 Countries. *CA: A Cancer Journal for Clinicians*, 71(3). <https://doi.org/10.3322/caac.21660>
- Surveillance Research Program. (2021). *SEER*Explorer: An interactive website for SEER cancer statistics*. National Cancer Institute.
- Théry, C., & Amigorena, S. (2001). The cell biology of antigen presentation in dendritic cells. *Current Opinion in Immunology*, 13(1), 45–51. [https://doi.org/10.1016/s0952-7915\(00\)00180-1](https://doi.org/10.1016/s0952-7915(00)00180-1)
- Ugai, T., Sasamoto, N., Lee, H. Y., Ando, M., Song, M., Tamimi, R. M., Kawachi, I., Campbell, P. T., Giovannucci, E. L., Weiderpass, E., Rebbeck, T. R., & Ogino, S. (2022). Is early-onset cancer an emerging global epidemic? Current evidence and future implications. In *Nature Reviews Clinical Oncology* (Vol. 19, Issue 10). <https://doi.org/10.1038/s41571-022-00672-8>
- Vázquez-García, I., Uhlitz, F., Ceglia, N., Lim, J. L. P., Wu, M., Mohibullah, N., Niyazov, J., Ruiz, A. E. B., Boehm, K. M., Bojilova, V., Fong, C. J., Funnell, T., Grewal, D., Havasov, E., Leung, S., Pasha, A., Patel, D. M., Pourmaleki, M., Rusk, N., ... Shah, S. P. (2022). Ovarian cancer mutational processes drive site-specific immune evasion. *Nature*, 612(7941). <https://doi.org/10.1038/s41586-022-05496-1>
- Vikas, P., Borchering, N., Chennamadhavuni, A., & Garje, R. (2020). Therapeutic Potential of Combining PARP Inhibitor and Immunotherapy in Solid Tumors. *Frontiers in Oncology*, 10. <https://doi.org/10.3389/fonc.2020.00570>
- Zhang, L., Conejo-Garcia, J. R., Katsaros, D., Gimotty, P. A., Massobrio, M., Regnani, G., Makrigiannakis, A., Gray, H., Schlienger, K., Liebman, M. N., Rubin, S. C., & Coukos, G. (2003). Intratumoral T Cells, Recurrence, and Survival in Epithelial Ovarian Cancer. *New England Journal of Medicine*, 348(3), 203–213. <https://doi.org/10.1056/NEJMoa020177>